ORIGINAL PAPER

Finite element modeling of thermomechanical problems under the vehicle braking process

Ali Belhocine[1] · Asif Afzal[2]

Abstract

The braking phenomenon is an aspect of vehicle stopping performance where in kinetic energy due to speed of the vehicle is transformed into thermal energy produced by the brake disc and its pads. The heat must then be dissipated into the surrounding structure and into air flow around the brake system. The thermal friction field during the braking phase between the disc and the brake pads can lead to excessive temperatures. In our work, we presented numerical modeling using ANSYS software adapted in the finite element method, to follow the evolution of the global temperatures for the two types of brake discs, full and ventilated discs, during braking scenario. Also, numerical simulation of the transient thermal analysis and the static structural were performed here sequentially, with coupled thermo-structural method. Numerical procedure of calculation relies on important steps such that the Computational Fluid Dynamics (CFD) and thermal analysis have been well illustrated in 3D, showing the effects of heat distribution over the brake disc. This CFD analysis helped us in the calculation of the values of the thermal coefficients (h) that have been exploited in 3D transient evolution of the brake disc temperatures. Three different brake disc materials were tested and comparative analysis of the results was conducted in order, to derive the one with the best thermal behavior. Finally, the resolution of the coupled thermomechanical model allows us to visualize other important results of this research such as the deformations and the equivalent stresses of von Mises of the disc, as well as the contact pressure of the brake pads. Following our analysis and results we draw from it, we derive several conclusions. The choice allowed us to deliver the rotor design excellence to ensure and guarantee the good braking performance of the vehicles.

Keywords Brake disc · CFD · Heat flux · Heat transfer coefficient · Pad · Gray cast iron · von Mises stress · Contact pressure

List of symbols

a	Vehicle deceleration (m/s^2)
A_c	Surface area of the braking pad (m^2)
A_d	Disc surface swept by a brake pad (m^2)
$[B]$	Kinematic matrix
C_p	Specific heat (J/kg °C)
$[D]$	Material property matrix
d	Displacement vector (m)
E	Young's modulus (MPa)
F	Force vector (N)
F_{disc}	Rotor force (N)
g	Gravitational acceleration (m/s^2)
h	Heat transfer coefficient (W/m^2 °C)
k	Thermal conductivity (W/m °C)
$[K]$	Stiffness matrix
m	Vehicle mass (kg)
p	Pressure (Pa)
P	Pressure for a single pad (MPa)
q_0	Heat flux entering the disk (W)
q_x	Conduction heat flux in x-direction (W/m^2)
q_y	Conduction heat flux in y-direction (W/m^2)
q_z	Conduction heat flux in z-direction (W/m^2)
Q	Internal heat generation rate per unit volume (W/m^3)
R_{rotor}	Effective rotor radius (m)
R_{tire}	Tire radius (m)
S_m	Source term (kg)
t	Time (s)
T	Temperature (°C)
T_1	Specified surface temperature (°C)
T_s	Unknown surface temperature (°C)

✉ Ali Belhocine
   al.belhocine.2018@gmail.com

1   Department of Mechanical Engineering, University of Sciences and the Technology of Oran, L.P 1505 El -MNAOUER, USTO, 31000 Oran, Algeria

2   Department of Mechanical Engineering, P. A. College of Engineering, Mangalore, India

t_{stop}	Time to stop (s)
T_e	Convective exchange temperature (°C)
v	Velocity vector (m/s)
v_0	Initial speed of the vehicle (m/s)
v_r	Relative velocity vector (m/s)
x	Space variable in x-direction (m)
y	Space variable in x-direction (m)
z	Space variable in x-direction (m)
z	Braking effectiveness

Greek symbols

α	Thermal expansion coefficient (1/°C)
ε	Strain vector
ε_p	Factor load distribution on the disk surface
μ	Coefficient of friction disc/pad
ρ	Mass density (kg/m³)
σ	Stress vector (N/m²)
τ	Stress tensor (Pa)
υ	Poisson coefficient
ϕ	Rate distribution of the braking forces between the front and rear axle
ω	Angular velocity (rad/s)
Ω	Angular velocity vector (rad/s)

Subscripts

CFD	Computational fluid dynamic
FG	Gray cast iron
HTC	Heat transfer coefficients
me	Mechanical index
th	Thermal index

1 Introduction

Automobile is complex integration of electronic and mechanical components. One of the major components is the braking system which is limited due to its shortcomings. The translational movement of the brake pedal needs to be converted into the rotational movement of the airfoil blade to increase drag during the braking process. The precise calculation of the total heat generated by the friction between the automobile brake disc and the brake pads, as well as the distribution of this heat energy, is an essential step in the thermal analysis of the automotive braking system. It is obvious, therefore, that the calculation of the heat transfer coefficient (h) in simulation and numerical modeling is very serious. Huajiang et al. (2004) presented a dynamic model for a disc subjected to two sliders rotating in the circumferential direction over the top and bottom surfaces of the disc. Liu et al. (2019) investigated the frictionally excited thermoelastic dynamic instability. Botkin (2000) provided design methodology of Carbon Fiber-Reinforced Composite Automotive Roof, including finite element analysis for realistic loading conditions, for specific major body component.

Kothawade et al. (2016) conducted numerical simulation using CFD analysis, to find the variations of the thermal transfer coefficients (h) during braking of the vehicle for each rotor area to exploit them in the search for the temperature reached in both disc designs (full and ventilated) while adapting the finite element method (FEM). In work done by Tang et al. (2014), and in the context of improving the accuracy of coupled computation techniques (CFD and FEM), modeling of the transient thermal transfer of brake disc was presented by the authors. Adamowicz and Grzes (2012) used the finite element method (FEM) in their study to clarify the effect of the convection transfer coefficient (h) around the full disc during its heat dissipation phase. Belhocine and Bouchetara (2012a, b) used the finite element software ANSYS 11.0 to study the thermal behavior of full and ventilated disc brake rotor. Belhocine et al. (2015) examined the stress concentration, structural deformation and contact pressure of the brake disc and pads during single braking stop event. Belhocine (2015) investigated the structural and contact behaviors of the brake disc and pads during the braking phase with and without thermal effects. Belhocine and Wan Omar (2018) studied the contact mechanics and behavior of dry slip between the disc and brake pads during the braking process. Ishak et al. (2018) developed one-dimensional (1D) model of leading–trailing drum-type parking brake model and then verified with experiments test bench. Belhocine and Nouby (2016) developed a finite element model of the whole disc brake assembly and validated using experimental modal analysis.

The main purpose of this scientific contribution is to present a numerical simulation during stop braking step to visualize the thermomechanical behavior of the automobile brake discs while considering the generation of an initial heat flow generated by friction between both parts in dry contact. This document is a guide to the physical presentation of thermomechanical coupling and even constitutes a separate report summarizing the articles previously published by the same author whose simulation characterization methodology is the subject of an extremely large and complex subject and whose computational strategy developed here and is, this time, exposed deeply for the impact of scientific contribution. The novelty of the present work is to obtain numerical solutions for thermomechanical behavior of disc brake assembly using finite element analysis software ANSYS under weak coupling. The results for various states are verified with known data in the literature. We focused first our intelligence on the actual evaluation of the values of Convective Heat Transfer Coefficients (HTC) as function of time, by adopting the ANSYS CFX code of which these have been used in the prediction of the transient temperatures of brake discs while seeing the performance of three gray cast irons. Thus, comparative results on temperatures of the two discs allowed us to get the best cooling style that

is used in the prototype of manufacture of automotive brake discs. These are then compared with experimental results obtained from the literature that measured ventilated disc surface temperatures to validate the accuracy of the results from this simulation model. This simulation allowed us to visualize some important results such as the global deformations and Von Mises stress of the model (disc–pads), the field of contact pressure of the inner pads as well as the influence of the brake pad groove and the mode of loading exerted by the piston on the stresses established on the structure. The results of this analysis are in accordance with reality and in the current life of the braking phenomenon and in the brake discs in service thus with the thermal gradients and the phenomena of damage observed on used discs brake.

2 Brake disc kinds

We know in the field of the automobile, two kinds of brake discs: full discs and ventilated discs. Full discs usually have a crown attached to bowl disc which is nailed to the wheel of the vehicle (Fig. 1a). Ventilated brake discs are modern discs of complex shape used in our time when they are equipped with front axles of vehicles by constituting two so-called broken crowns which are separated by fins (Fig. 1b).

3 Numerical simulation methodology

The disc brake heat transfer problem was analyzed using a coupled CFD/FEA simulation method. The CFD analyses for this study were performed in ANSYS CFX. The primary purpose of the CFD analysis was to compute the
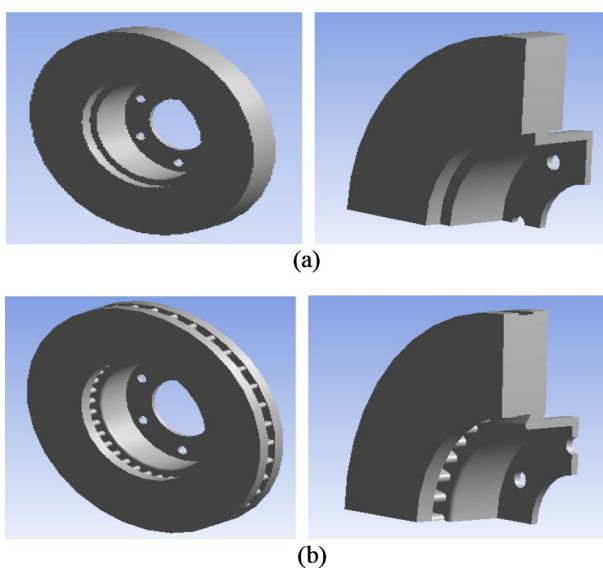

(a)

(b)

Fig. 1 CAD model of discs brakes: **a** full disc, **b** ventilated disc

HTCs on the solid boundaries. Because heat transfer coefficients (HTCs) are dependent on temperature, it was necessary to couple the CFD and FEA solutions. These produced HTC vs. time curves. An iterative process of transferring HTCs from CFD to FEA was developed. The temperature distribution of the disc brake rotor was calculated using the FEA model. In our case, where the thermal and mechanical problems are decoupled, it is advisable to resort to a weak coupling resolution consisting of first determining the temperature field independently of the mechanical conditions and then evaluating the stresses and deformations induced by this field temperature. The step by step process of solving a coupled thermomechanical problem is highlighted as a flowchart in Fig. 2.

4 CFD modelling and analysis with ANSYS CFX

4.1 Governing equations

The model we found here in this study is similar to that developed by Palmer et al. (2009). All equations used in CFD analysis, namely the Navier–Stokes moment equation, the energy equation, and the continuity equation, were used to solve the thermal problem, which is the variation of heat transfer and air flow around the brake disc.

4.1.1 Continuity equation

The conservation equation of mass in the case of compressible and incompressible fluids is defined as follows:

$$\frac{\partial \rho}{\partial t} + \nabla \cdot (\rho u) = S_{\mathrm{m}}, \tag{1}$$

where S_{m} is the mass added to the continuous phase from the dispersed second phase.

4.1.2 Momentum (Navier–Stokes) equations

In inertial frame, the general equation the conservation of momentum is given by the form:

$$\frac{\partial (\rho v)}{\partial t} + \nabla \cdot (v v) = -\nabla p + \nabla \cdot (\tau) + \rho g + F, \tag{2}$$

where the stress tensor τ is of the form:

$$\tau = \pm \mu \left[(\nabla v + \nabla v^{T}) - \frac{2}{3} \nabla \cdot vI \right]. \tag{3}$$

The left term of Eq. (2) can be reduced to the form below using the rotating reference frame (RRF) technique in the case of rotating brake disc and in absolute speed:
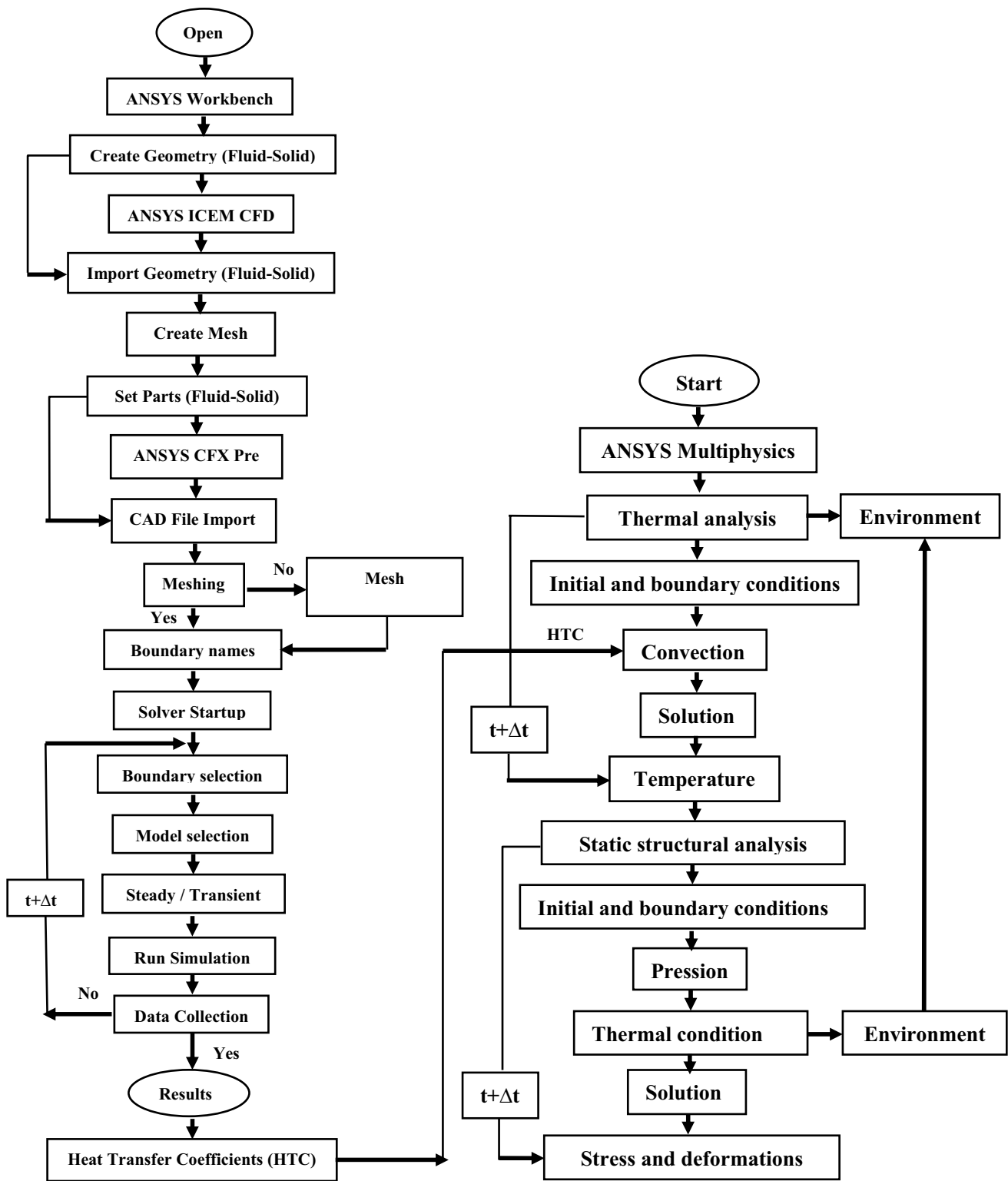
Fig. 2 Flowchart of present methodology

$$\frac{\partial\,(\rho v)}{\partial t} + \nabla \cdot (\rho\, v_r\, v) + \rho(\Omega \times v), \qquad (4)$$

where, Ω and v_r are, respectively, the angular velocity and the absolute velocity; the continuity equation used in analysis (RRF) is expressed as

$$\frac{\partial \rho}{\partial t} + \nabla \cdot (\rho v_r) = S_m. \tag{5}$$

4.2 Heat flux entering the disc

The general formula for calculating the initial flux entering the automotive brake disc can be expressed as follows (Reimpel 1998):

$$q_0 = \frac{1 - \varphi}{2} \frac{m \, g \, v_0 \, z}{2 \, A_d \, \varepsilon_p}, \tag{6}$$

where g is the acceleration of gravity (9.81) [ms^{-2}], a is the deceleration of the automobile [ms^{-2}], and $z = a/g$ is the braking efficiency.

The quantity evaluated using Eq. (6) of the initial heat flux has been exploited of course in the first step of the CFD analysis, and then in transient thermal analysis using finite element software (FE) ANSY Workbench 11.0 to visualize variation of the brake disc temperature.

Given the complexity of the phenomenon treated, we assumed that the thermal flux entering the rotor, and the brake pads replace the effect of dry friction between the two bodies in contact, as shown in Fig. 3. Until now, we focus on the transient thermal analysis of the brake disc. The thermomechanical coupling that we will discuss later is called weak coupling, where the resolution is sequential. We only take into account the effects of expansion, that is to say, the effects of the thermal on the mechanics. In other words, a thermal calculation is carried out followed by a mechanical computation with a fixed geometry. The investigations demonstrated that the geometry of a brake rotor has significant impact on its ability to dissipate heat via convection.
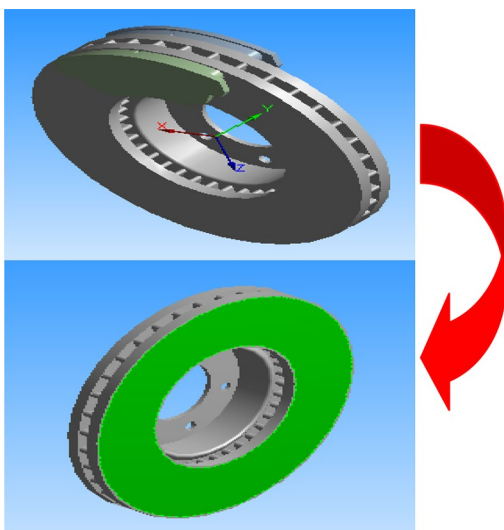

Fig. 3 Heat flux from braking friction

However, extensive complexity is required because of the brake rotor rotation, if the local convection HTCs from the fluid domain must be directly coupled with a solid domain. The coupling of mechanical and thermal thus impacts the results of HTC.

4.3 k–ε turbulent model

The turbulence model (k–ε) is the most widely used model in the field of CFD analysis as numerical simulation of the average flow characteristics in the turbulent flow regime. For current models, the model provides a good agreement for accuracy and virility.

4.4 Modelling assumptions

For us to facilitate CFD analysis calculations, we have introduced the assumptions that are summarized as

- the flow medium is air;
- the vehicle starts with initial speed of 28 m/s
- the pure nature of the fluid in calculation is air,
- the air inlet speed is fixed at 28 m/s;
- the regime is steady-state turbulent incompressible flow around the disc brake rotor according to the turbulence model k–ε;
- the thermo-physical properties taken into calculation are constant (viscosity, specific heat, thermal conductivity, and density);
- the radiation phenomenon is neglected whereas only conduction and thermal convection are considered here;
- the distribution of heat flux on area of the brake disc is quite uniform;
- under normal pressure and temperature conditions, the physical properties of the air are considered;
- heat flux is uniform over pad area;
- brake disc absorbs almost 90% of thermal friction.

4.5 CFD analysis with ANSYS CFX

Various external and internal faces of the two structures, full and ventilated discs, that were derived from the code ANSYS ICEM CFD are shown in Figs. 4 and 5. In these figures, all the external and internal surfaces have been chosen because the values of the thermal transfer coefficient are practically dependent on the factor of the geometric design of the disc.

The mesh is realized here in linear tetrahedral elements with 179,798 elements and 30,717 nodes (Fig. 6). ANSYS-CFX code solves the CFD aerodynamic model of the brake disc while basing on transitory type of the problem whose all boundary conditions were injected in both domains (solid and fluid).
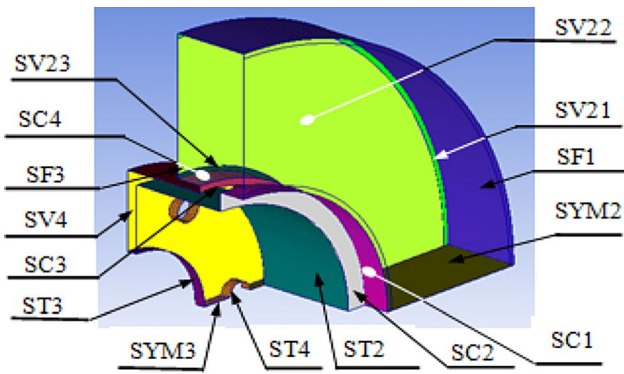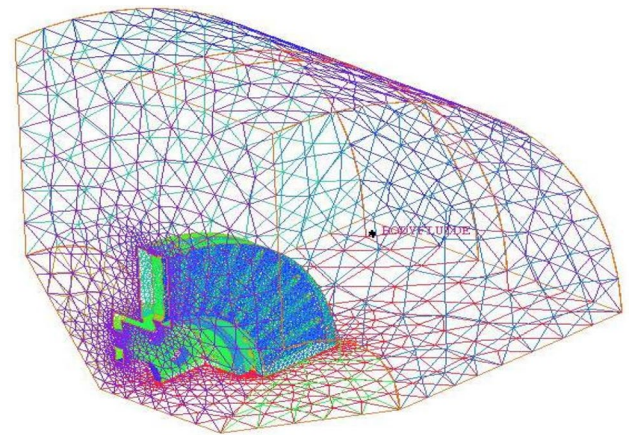
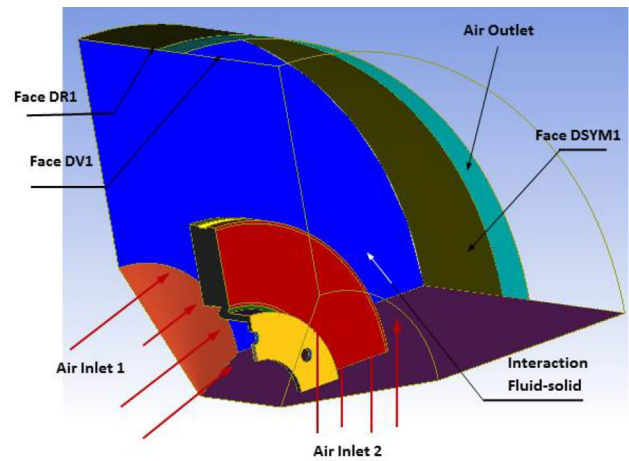**Fig. 4** Quarter of full disc showing the assignment of face names in the simulation
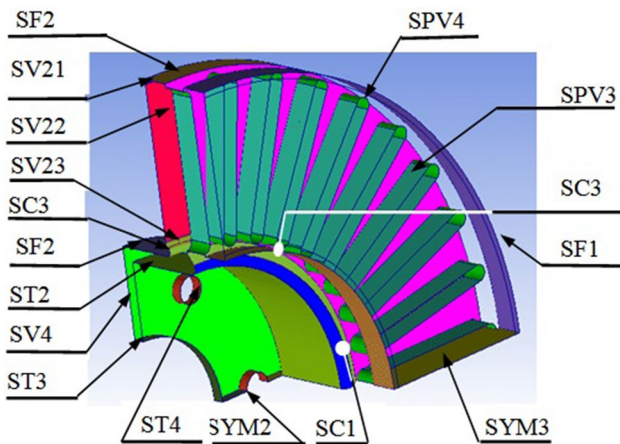
Fig. 5 Quarter of the ventilated disc showing the assignment of face names
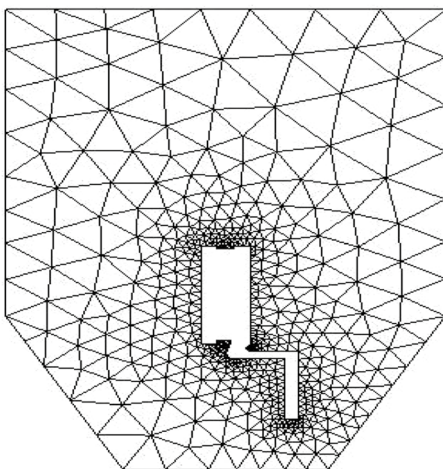
Fig. 6 Wall meshes for the CFD simulation

Fig. 7 Meshing for a fluid body

Fig. 8 Fluid body surfaces in ANSYS ICEM CFD

In this study, we have considered that the temperature of ambient air 20 °C surrounding the brake disc is equal to it in the initial state, zero relative pressure of which has been maintained at the high, low and radial terminals of the fluid domain.

4.6 Fluid mesh generation

In this study, the size of the fluid body is $1.95e^{-7}$ mm^3, and the mesh generated on the model characterizing the fluid domain is tetrahedral mesh containing 179,798 elements and 30,717 nodes, as shown in Fig. 7.

Due to symmetrical shape of the brake disc, we modeled only a quarter of the fluid domain geometry using ANSYS ICEM CFD software which gives us the graphical interface shown in Fig. 8.

4.7 Boundary conditions and computational details

In the present study, we have selected three types of gray cast iron materials used in the design of brake discs to study their performance; in this case, gray cast irons (FG25AL, FG20, FG15). CFD model developed in ANSYS CFX used in search for exchange coefficient values (h) is well shown in Fig. 9.

5 Finite-element modelling

5.1 Modelling assumptions

The standard dimensions of the full and ventilated brake discs are identical in this numerical simulation to ensure a better comparison of the results. Table 1 lists all the physical parameters and the geometric dimensions of the brake disc used in numerical calculations.
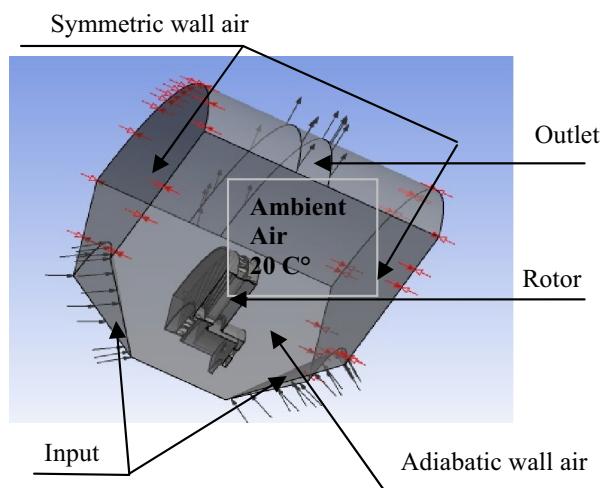
The material of the brake disc that we have opted for in this simulation having carbonaceous assembly is gray cast iron (FG15) (Gotowicki et al. 2005), which has excellent tribological and thermomechanical properties. We consider brake pads having a material characterized by purely isotropic elastic behavior whose properties of the two parts involved are explained in Table 2.

Research investigations showed the difficulty to actually model rotating brake disc, due to simultaneous interaction of several tribological and vibro-thermomechanical phenomena during automobile braking. Series of reasoning hypotheses have been applied here, throughout the duration of the braking (Khalid et al. 2011). These assumptions which are made while modeling the process are given below.

Table 1 Design parameters of brake disc

Parameter	Value
Inside diameter of the disc, mm	66
Outside diameter of the disc, mm	262
Disc thickness (TH), mm	29
Disc height (H), mm	51
Weight of the car m, kg	1385
Initial velocity v_0, m/s	28
Deceleration a, m/s^2	8
Time of braking t_b, s	3.5
Effective disc radius R_{disc}, mm	100.5
Ratio braking forces distribution ϕ, %	20
Factor of disc charge distribution ε_p	0.5
Disc's swept area A_d, mm^2	35993

- In this simulation, two modes of heat transfer by conduction and convection are considerable in internal and external faces of the brake disc in such way that the radiation exchanges are negligible (Limpert 1999).
- The kinetic energy of the vehicle which is dissipated during the braking mechanism is totally converted into heat energy represented by a heat flux distributed on the faces of the brake disc.
- The kinetic energy of the vehicle is lost through the brake discs, i.e., no heat loss between the tire and the road surface and deceleration is uniform.
- The initial temperature of the disc is constant and is equal to the air temperature of the environment at 20 °C.
- The physical properties of the brake disc material are isotropic and homogeneous and their thermal properties are dependent on temperature.
- During the braking time, the inertia and all other forces are considered negligible.
- The domain is considered as axis-symmetric.
- Brake distribution is 60% on front and 40% on rear.
- Force distributed on one brake disc is equal to the total frictional force applied on rubbing surface.
- Before the braking phase, the brake disc is free of any stress.

Table 2 Properties of the disc and pad

Material properties	Disc	Pad
Thermal conductivity, k (W/m °C)	57	5
Volumetric mass density, ρ (kg/m^3)	7250	1400
Specific heat capacity, c (J/Kg. °C)	460	1000
Poisson's ratio, v	0.28	0.25
Friction coefficient, μ	0.2	0.2
Young modulus, E (GPa)	138	1

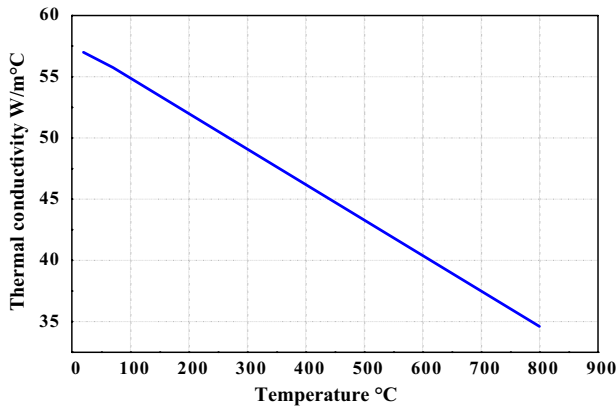**Fig. 9** CFD model of ventilated disc brake

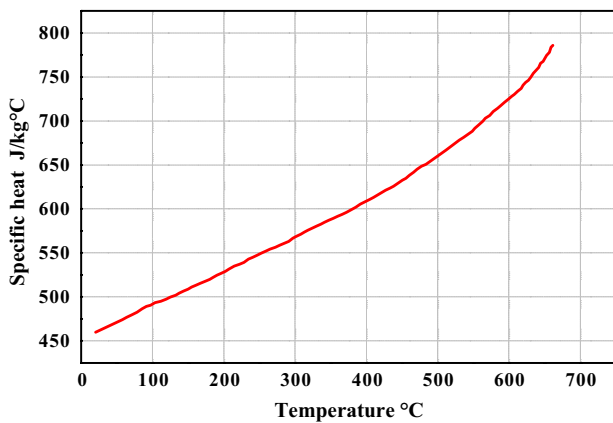**Fig. 10** Thermal conductivity versus temperature

Fig. 11 Specific heat capacity versus temperature

- All parts of the brake disc are subject to the phenomenon of thermal convection such as the outer ring diameter area, the outer ring diameter area, the cooling fins, and the disc brake surface.

Conductivity as well as specific heat capacity of the brake disc material are varied with temperature as shown in Figs. 10 and 11.

5.2 Auxiliary equations

The general three-dimensional heat transfer equation in iso-tropic material in Ω domain is given as follows:

$$-\left(\frac{\partial q_x}{\partial x} + \frac{\partial q_y}{\partial y} + \frac{\partial q_z}{\partial z}\right) + Q = \rho c \frac{\partial T}{\partial t} dx\,dy\,dz \quad (7)$$

where $T(x, y, z, t)$ is the temperature field, ρ is the density, C, is the heat capacity, $Q = Q(x, y, z, t)$ is the internal thermal energy by unit of volume, q_x, q_y and q_z are, respectively, the surface unit heat flux along the x-, y- and z-directions,

We can define like this, the thermal fluxes according to the directions of the axes x, y and z according to the Fourier law:

$$\begin{cases} q_x = -k\dfrac{\partial T}{\partial x} \\ q_y = -k\dfrac{\partial T}{\partial y}, \\ q_z = -k\dfrac{\partial T}{\partial z} \end{cases} \quad (8)$$

where k is the thermal conductivity. By substituting Eqs. (8) in (7), we obtain the following differential equation, which varies as function of temperature T:

$$\frac{\partial}{\partial x}\left(k\frac{\partial T}{\partial x}\right) + \frac{\partial}{\partial y}\left(k\frac{\partial T}{\partial y}\right) + \frac{\partial}{\partial z}\left(k\frac{\partial T}{\partial z}\right) + Q + \rho c \frac{\partial T}{\partial t} dx\,dy\,dz = 0. \quad (9)$$

The boundary conditions imposed on our thermal problem are expressed as follows.

- Temperature of fluid that enters the domain is based on the value specified temperature.

$$T_S = T_1(x, y, z, t) \text{ on } S_1. \quad (10)$$

- Heat flux is controlled by the temperature gradient and always flows from high-temperature regions to lower temperature regions.

$$q_x n_x + q_y n_y + q_z n_z = -q_s \text{ on } S_2. \quad (11)$$

- Convection is a group of thermal boundary conditions in which heat flow is a function of convection.

$$q_x n_x + q_y n_y + q_z n_z = -h(T_s - T_e) \text{ on } S_3, \quad (12)$$

where h is the convective exchange coefficient, T_e is the convection surface temperature, and T_s is temperature unknown to the S area. Knowledge of the initial temperature field at the time ($t = 0$) for any transient modeling is mandatory.

$$T(x, y, z, 0) = T_0(x, y, z). \quad (13)$$

5.3 Thermal loading applied to the disc

In this research work, we carried out numerical modeling of the transient thermal transfer in disc brake, by finite element method in which the type of braking of the adopted vehicle is that of emergency stop braking. The speed of the vehicle decreases linearly as a function of time until the moment of

braking ($t = 3.5$ s), stabilizing at the value zero until the end of this braking at the instant ($t = 45$ s), as shown in Fig. 12.

The heat flux is identified here as the thermal load which is generated by dry friction between the brake disc and the pads during the braking phase. At first, the value of this flow is maximum and it then decreases linearly until it vanishes at the end, as shown in Fig. 13.

5.4 Mesh of disc brake model

The application of generated mesh of brake disc in numerical modeling is useful from which one has chosen automatic mesh. On both brake disc friction tracks where the brake pads are turning, refined tetrahedral mesh has been performed on the ANSYS Multiphysics.

The final mesh, therefore, comprises 172,103 nodes and 114,421 elements for the full disc, and 154,679 nodes and 94,117 elements for the ventilated disc, as it is represented in Fig. 14.

5.5 Boundary conditions applied to the model

Modeling requires discretization of the time axis. Unlike numerical control, the discretization of the time axis does not have to be regular. The parameters of the initial, minimum and maximum and final time increment for the simulation shall be inserted at the values (0.25 s, 0.125 s, 0.5 s, 45 s), respectively, maintaining the initial temperature of the disc at 20 °C. The values of the convection exchange coefficient (h) for each face of the brake disc must be imported from CFX analysis results and must be used in the ANSYS Workbench Multiphysics analysis. These are shown in the following in the graphs of Fig. 20. The imposed heat flux on the lateral surfaces corresponds to their values resulting from the CFX analysis.
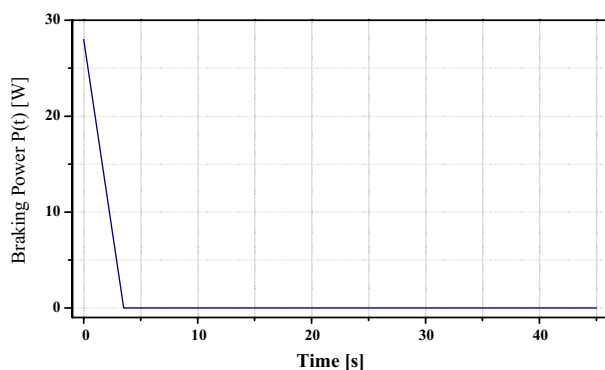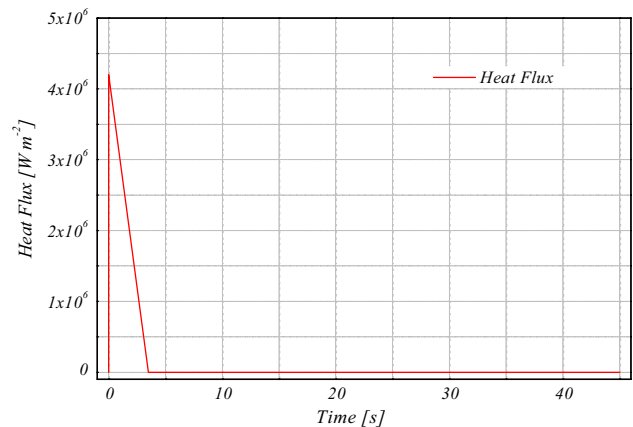

Fig. 13 Heat flux versus time

6 Experimental setup

The numerical results of the thermal simulation obtained in this work using ANSYS are validated using the results of the work of Stephens (2006), which was an experimental investigation on temperature distribution of ventilated disc brake rotor.

6.1 Temperature measuring with embedded thermocouple

The temperature measurement was conducted using Cu thermocouples integrated in the disc brake rotors according to VDA285-1, which became accredited until the year 1996, at the mean friction radius as shown in Fig. 15a. The temperature pot-side was measured also by Cu-embedded thermocouple as shown in Fig. 15b. The thermocouples have a cylindrical shape in this case with the sizes $\varnothing = 3$ mm and $h = 3$ mm as in Fig. 15c. The connecting wires were insulated on the brake rotor side and were connected to the signal amplifier.
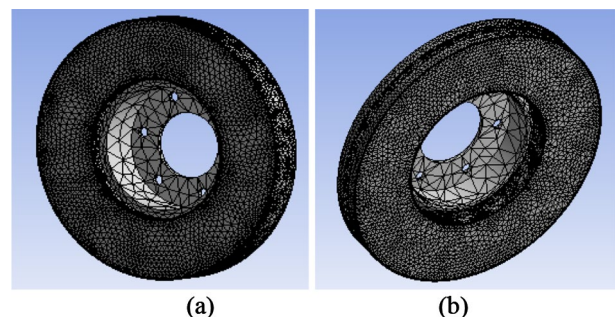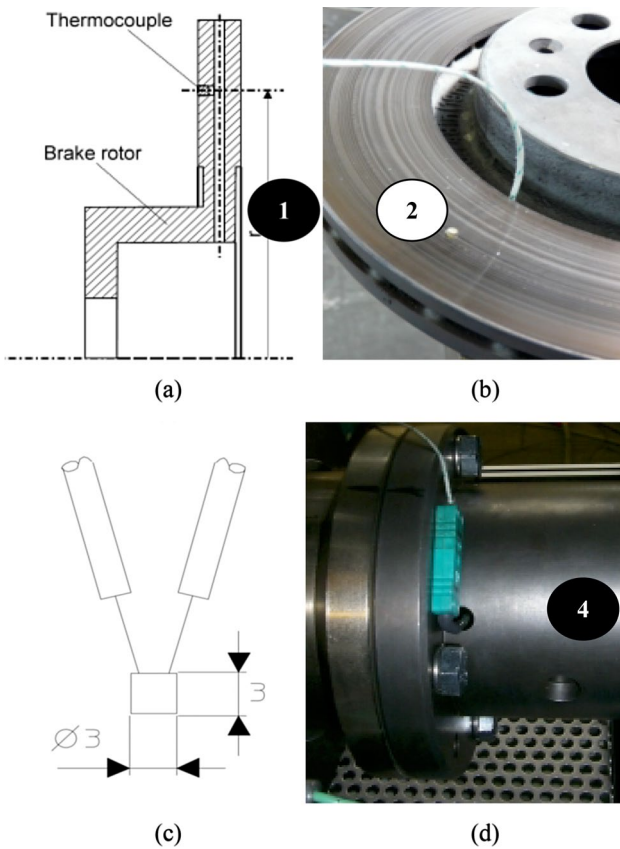

Fig. 12 Braking power versus time

Fig. 14 Disc brake mesh model: **a** full disc, **b** ventilated disc

Fig. 15 Temperature measuring with embedded thermocouple as per VDA285-1
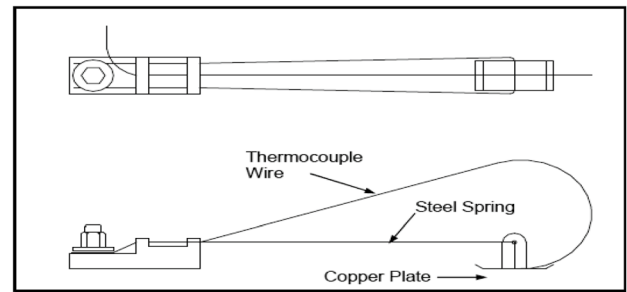
6.2 Disc brake thermocouples

Thermocouples are the favored choice for testers due to their cost, ease of use and availability, and are one of the most stable methods of measuring the temperature of disc brakes in vehicles with rubbing disc brakes. The device contains K-type thermocouple, which is made using silver wire welded to a flat piece of copper plate, and this plate is strongly supported against the rotating disc by a steel spring. Elementary diagram of the thermocouple is provided in Fig. 16.

6.3 Experimental procedure

The brake was connected to the external applicator and the right rear wheel of the racing vehicle was fitted in the brake test rig as shown in Fig. 17. The rubbing thermocouple was positioned to measure the temperature on the inner surface of the rotor. The thermocouple data were recorded in the PC via a Fluke data logger.

The tests were performed by rotating the wheel at constant speed approximately equal the vehicle speed of 108 km/h. Progressive braking load was applied and the temperatures were

Fig. 16 Diagram of disc brake thermocouple

recorded at very short intervals of 0.01 s. The method started with the disc heating up to temperature of about 345 °C, at which point the braking load was released. The recording continued there on until the temperature of the rotor dropped to about 200 °C. The results of the thermocouple readings were obtained directly from the PC in temperature scale.

7 Results and discussion of CFD analysis

7.1 Steady-state cases

The results obtained from the distribution of the wall heat transfer coefficient of the two of the discs in the stationary state are illustrated in Figs. 18 and 19.

Table 3 lists the average heat transfer coefficients of the named surfaces in the CFD model of full brake disc made of the material FG15.

The distribution of the heat transfer coefficient to the wall (h) according to the three types of brake disc materials is well represented in Fig. 19a–c. It is observed that the variation of (h) in the brake disc does not subordinate to the material and that this one is not the same one found in the specialized literature.

From the maximum and minimum values of the various areas of the ventilated brake disc, the average values
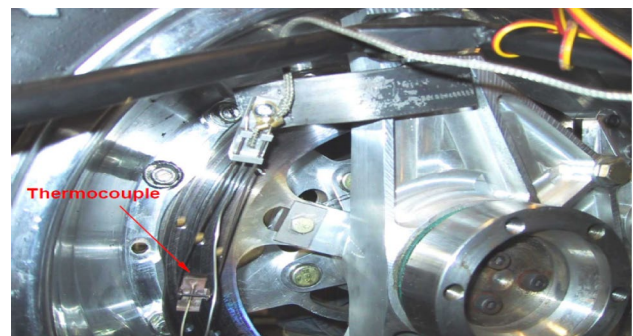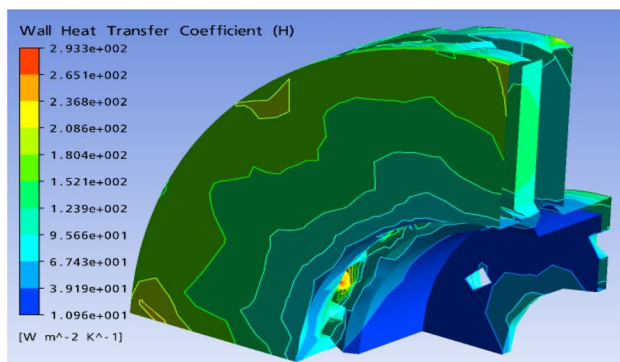

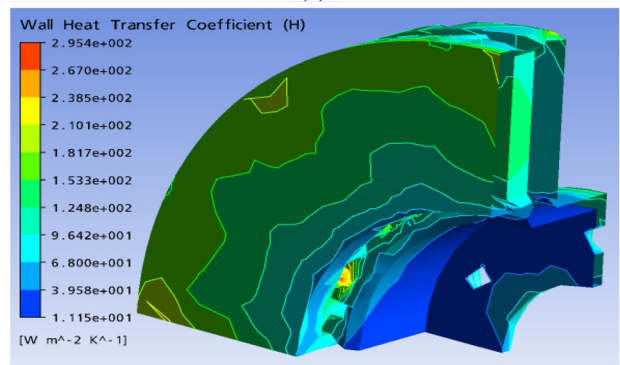**Fig. 17** Close-up view of thermocouple in position
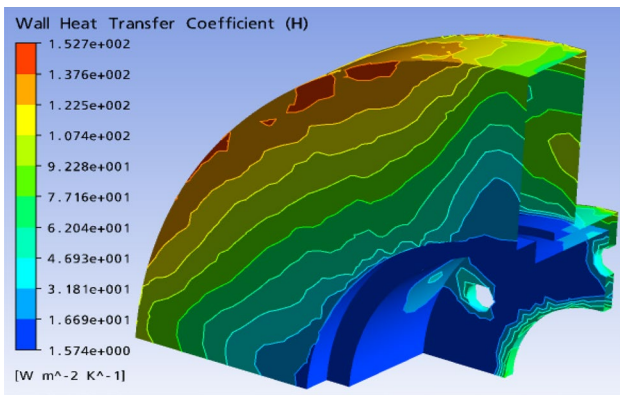
Fig. 18 Values of heat transfer coefficient at the wall of the full disc with material FG15 in steady-state thermal analysis

(a)

(b)

(c)

Fig. 19 Values of heat transfer coefficient at the wall of the ventilated discs with materials: **a** FG25 AL, **b** FG20 and **c** FG15 in steady-state thermal analysis

Table 3 Values of the wall heat transfer coefficients of different surfaces in the steady-state case for a full disc with material FG15
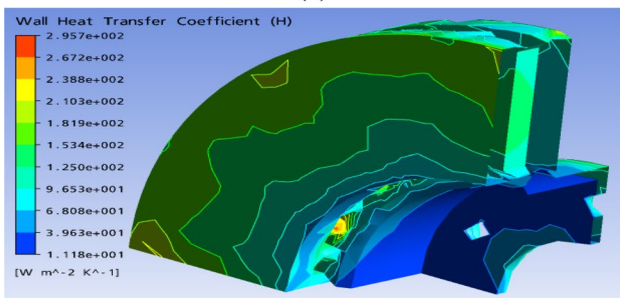
Surface	Material FG15 $h_{\text{average}} = [\text{W m}^{-2} \text{ k}^{-1}]$
SC1	25.29168
SC2	5.18003
SC3	2.922075
SC4	11.77396
SF1	111.20765
SF3	53.15547
ST2	23.22845
ST3	65.6994
ST4	44.26725
SV1	81.37535
SV2	71.75842
SV3	41.83303
SV4	65.82545

Table 4 Values of the wall heat transfer coefficients of different surfaces in steady-state case for ventilated discs with materials FG25 AL, FG20 and FG15

Materials Surface	FG25 AL $h_{\text{average}} = [\text{W m}^{-2} \text{ k}^{-1}]$	FG20	FG15
SC1	54.1624	53.9260	53.8749
SC2	84.6842	83.7842	83.6516
SC3	44.4171	44.3485	44.3295
SF1 and 2	135.4039	135.0584	135.0007
SF3	97.1710	95.0479	94.8256
SPV1	170.6472	171.4507	171.5696
SPV2	134.0815	134.3285	134.3615
SPV3	191.2441	191.9436	192.0391
SPV4	175.1667	176.13340	176.2763
ST1	113.6098	114.3962	114.3916
ST2	35.0993	34.4723	34.3473
ST3	68.3316	66.3316	66.0317
ST4	75.0945	72.1235	71.6642
SV1	135.5299	131.1183	131.2075
SV2	119.2572	118.4648	118.2040
SV3	46.7023	44.8195	44.5264
SV4	111.5769	108.5044	108.1817

of the heat transfer coefficient can be taken from the wall (*h*). The average values of each face in Table 4 have been obtained by selecting in the code, the surface S that one wishes to calculate its coefficient (*h*), the software ANSYC CFX Post records during the simulation two values (maximum and minimum) of the wall heat transfer coefficient (*h*) is located to the left of Fig. 19 at the top and bottom, respectively. We divide by two, the sum of the maximum and minimum value, so we get the average value that is reported in Table 4. These harvested data are grouped

together in Table 4. From the observation, it can be seen that there is no significant variation in this coefficient (*h*) when changing the material of the brake disc. Contrary to what we have seen, the heat transfer coefficient values at the wall are much more influenced by the ventilation system of the brake disc for the same material (FG15).

7.2 Transient cases

7.2.1 Evaluation of the heat exchange coefficient (*h*)

In transient situation, this convective heat exchange coefficient (h) is variable as a function of time on each disc surface (Zhang and Xia 2012). This one, practically, has nothing to do with the material, but it depends on the surface geometry as well as the conditions of law of the convective regime.

Figure 20a, b shows the evolution of the heat transfer coefficient (*h*) at each surface of the full and ventilated disc, as function of time. We used these two graphs later to predict the three-dimensional distribution of the two brake discs. It can be said that the values of the convective heat exchange coefficient (*h*) vary according to the geometric design of the disc, whether it is full or ventilated and, it is quite rational that the aeration generates the decrease of the maximum temperatures at the walls. The variations of the wall heat transfer coefficient as a function of time for insulated surfaces SV1 and SPV2, respectively, belong to the full and ventilated brake disc for material FG15 are clearly shown in Fig. 21a, b.

8 Results and discussion of FEM analysis

8.1 Model validation against experimental data

The analysis in this work is compared to available literature to ensure the reliability of the results. Figure 22 shows the time variation of the observed disc temperature against the values from Stephens (2006). Figure 22 shows that the temperature results from both the thermocouple and the finite element software ANSYS 11.0 of the ventilated disc brake made of material FG15 are very similar. It is believed that the response of the thermocouple is a little slower in cooling than heating due to residual heat in its rubbing components. But the variation is small as shown in the figure, such that it was decided that the level of accuracy of rubbing type thermocouples used in the experimental stages of this research is acceptable. It can also be concluded that the transient thermal simulation of the ventilated disc, performed by the finite element method, gives us a good correlation with the thermocouple measurements.
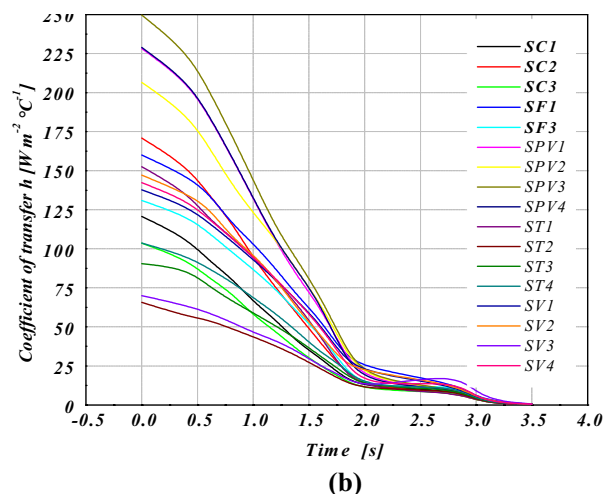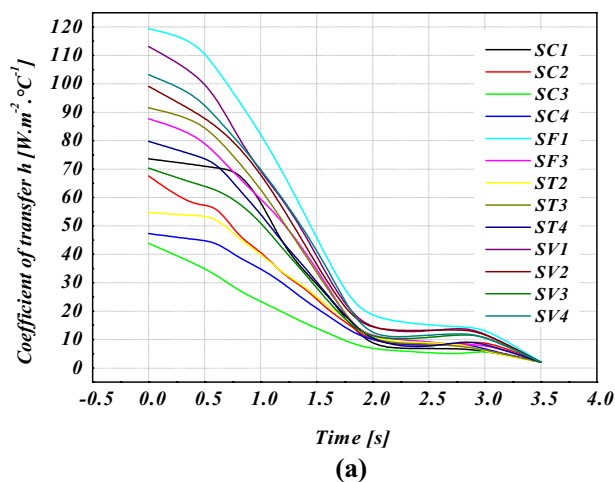

Fig. 20 Heat transfer coefficient (*h*) versus time at different disc surfaces at material FG15 in transient thermal case for **a** full disc faces, and **b** ventilated disc

8.2 Results of the disc temperature

The transient thermal analysis of the two discs, full and ventilated brake discs were performed using finite element (FE) software. The calculation does not last very long, which is a positive point. The results of the temperature distribution (3D) for the three materials, namely the gray cast iron FG25AL, FG20, and FG15, are provided in Fig. 23. It should be understood that the material having lower thermal conductivity thus generates important thermal gradients and consequently increase in the surface temperature of the brake disc. To make the choice of material and to know if it is profitable, we tested the one that cools better, it is necessary to remember that one wants to have material which does not preserve the heat. From the results provided by this simulation, it can be seen that the ventilated discs made
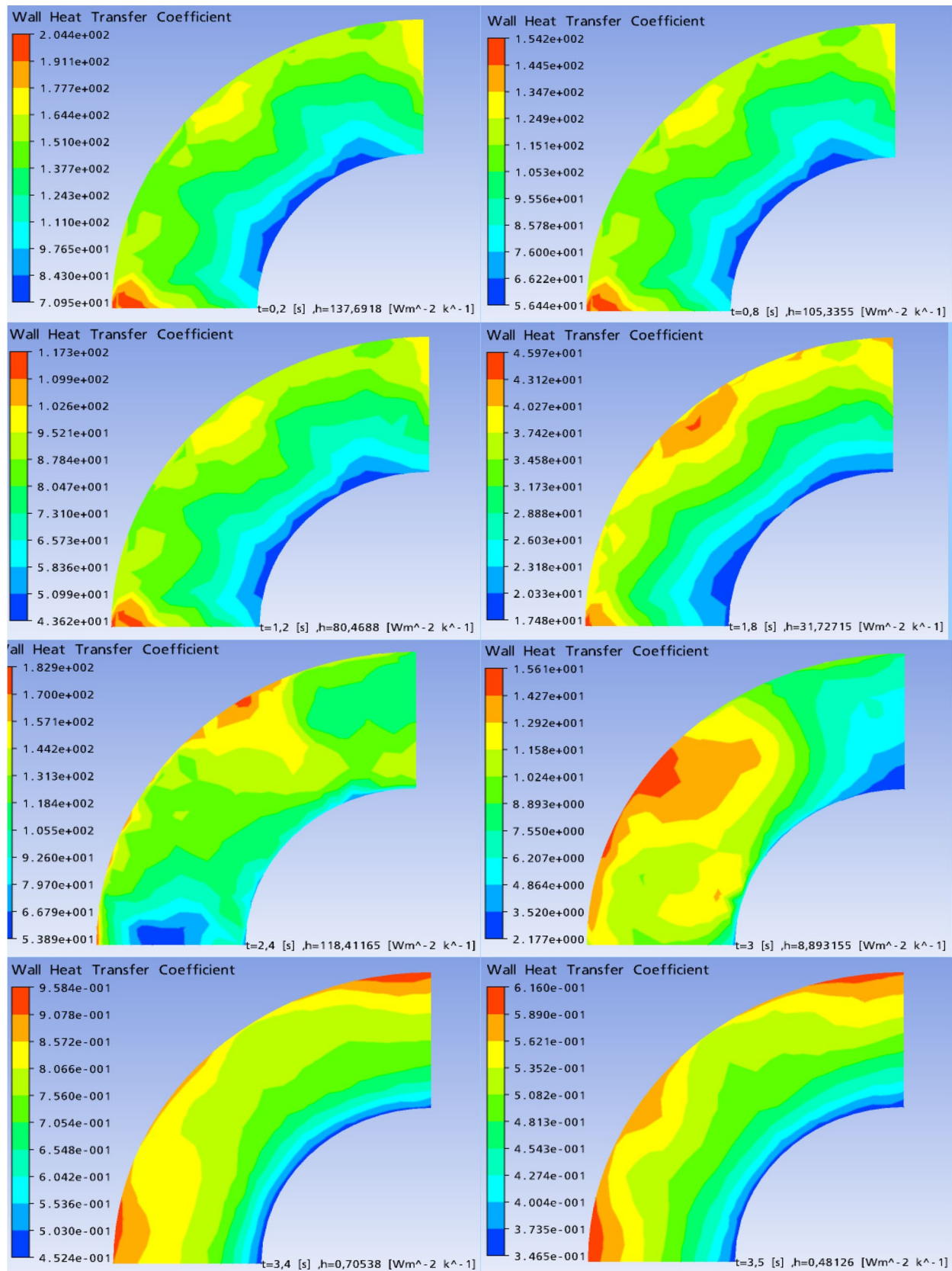
(a)

Fig. 21 Variation of the heat transfer coefficients (*h*) in specific time sequence of the discs with FG15 material. **a** Surface SV1 of the ventilated disc and **b** surface SV2 of the full disc
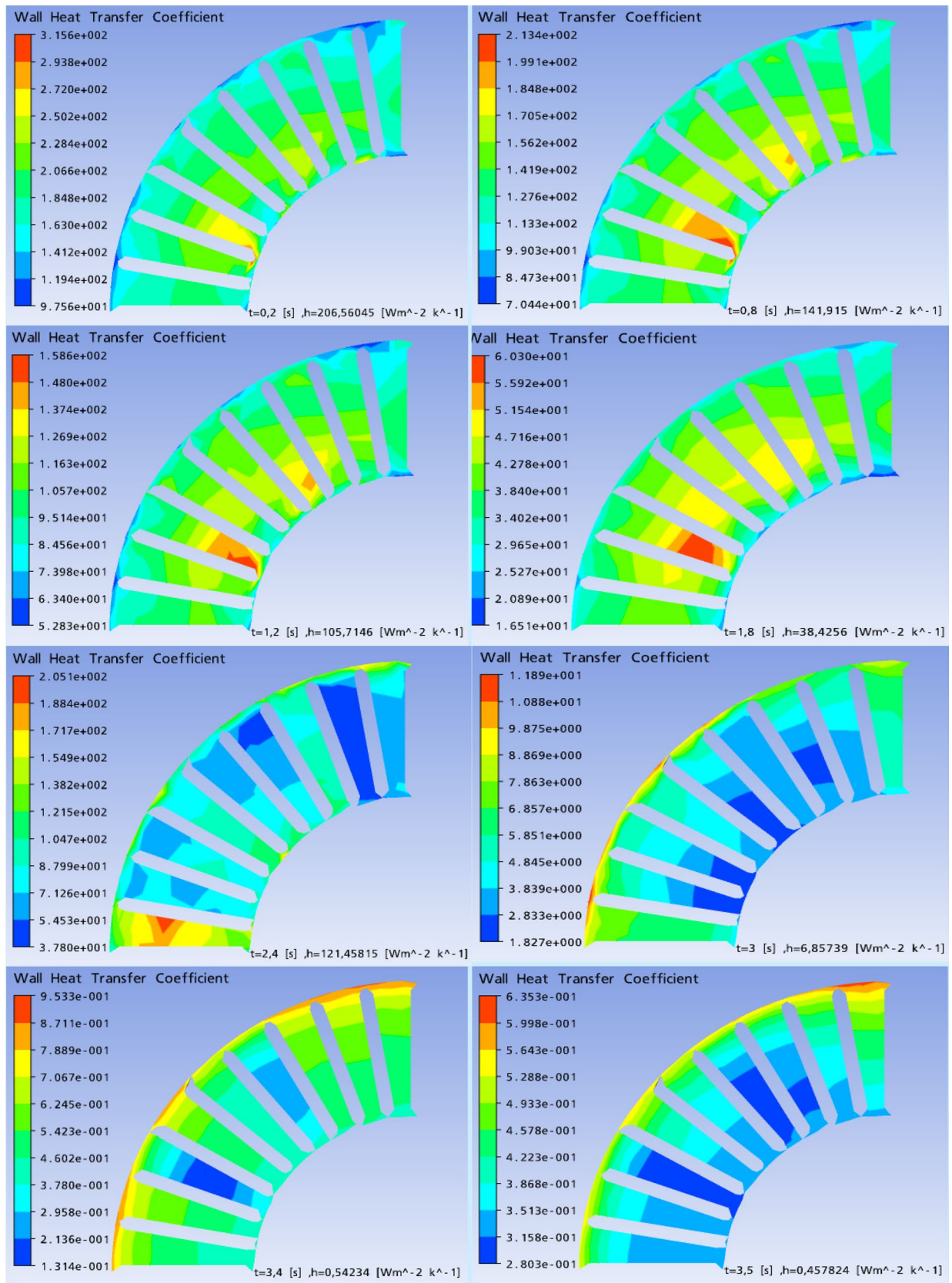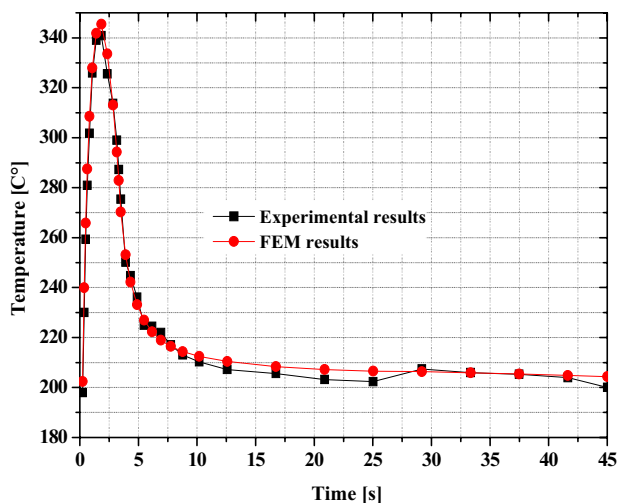
(b)

Fig. 21 (continued)

Fig. 22 Validation of the FEM model against experiments by Stephens (2006)

Fig. 23 Temperature plot of ventilated discs for three materials gray cast iron **a** FG25 AL, **b** FG20, and **c** FG15

of the materials FG20 and FG25AL, respectively, having temperatures reaching 351.5 and 380.2 °C, which in turn are greater than that of the ventilated disc of material FG15 having a maximum temperature of 345.4 °C as indicated in Fig. 24. It can thus be concluded that the most suitable material in this case for the brake discs is the gray cast iron FG15 which presents the better thermal performance.

Figure 25 shows the temperature of the brake disc at time $t = 1.8$ s reaching maximum value of 401.5 °C, and after that, it decreases exponentially at 4.9 s until it reaches braking cycle termination at instant, $t = 45$ s. The forced convection step is well designated in the temporary interval between the instant 0 s and 3.5 s, as shown in Fig. 25. On the other hand, the natural or free convection is quite marked after the duration of the forced convection arriving at the end of braking time, which is the total time of the simulation ($t = 45$ s). It can be seen from the graphs that the temperature of the full brake disc exceeds that of the ventilated disc with difference of 60 °C. Finally, we can draw the conclusion that the ventilated brake disc allows us to provide better cooling; therefore, better endurance and gives us ability to dissipate more heat for braking efficiency.

9 Coupled thermomechanical analysis

9.1 Calculation of hydraulic pressure

To proceed with the preliminary mechanical calculation, we determined the constant value of the hydraulic pressure exerted by the piston on the inner brake pad. For this, we
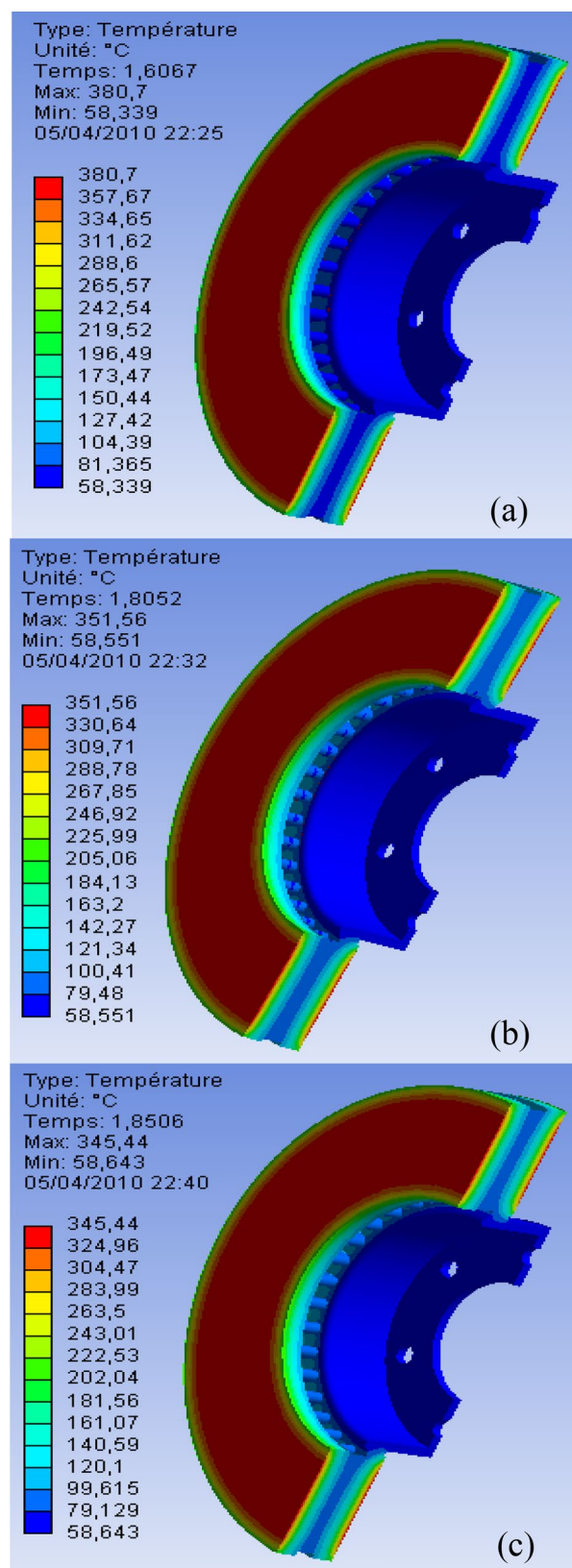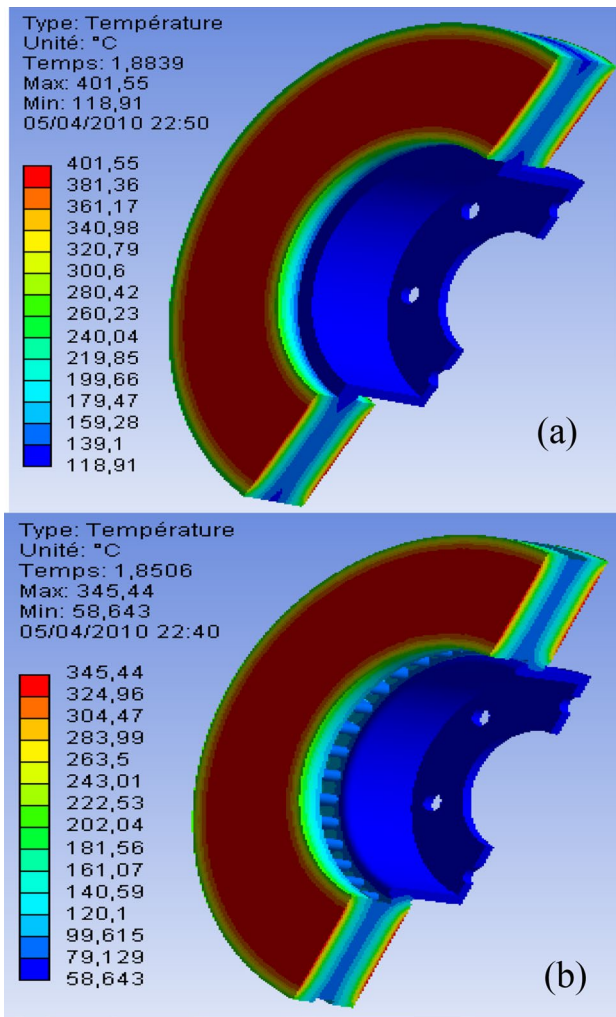
Fig. 24 Temperature plot on disc brake of the same material (FG15): **a** full disc, **b** ventilated disc

Fig. 25 Disc temperature versus time for **a** full disc and **b** ventilated disc, for material gray cast iron FG15

Table 5 Vehicle data

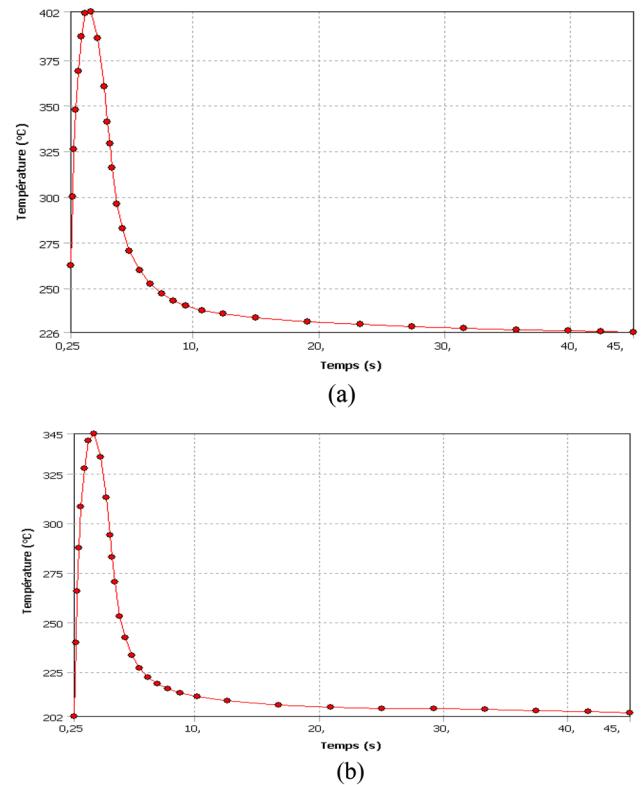| Item	Value
Vehicle mass—m (kg)	1385
The initial velocity—v_0 (m/s)	60
Duration of braking application (s)—t_{stop}	45
The effective radius of the disc—(mm)	100.5
The radius of the wheel—(mm)	380
Friction coefficient disc–pad μ (/)	0.2
Pad surface A_c [mm^2]	5246.3

assumed that the rate of 60% of the braking forces is maintained both front brake discs, giving a percentage of 30% for each rotor (Mackin et al. 2002). So, using the data in Table 5, we can thus calculate the typical force of a single rotor as follows:

$$F_{\text{disc}} = \frac{(30\%)\,\frac{1}{2}m v_0^2}{2\,\frac{R_{\text{rotor}}}{R_{\text{tire}}}\left(v_0 t_{\text{stop}} - \frac{1}{2}\left\{\frac{v_0}{t_{\text{stop}}}\right\} t_{\text{stop}}^2\right)} = 1047.36\ [N].$$
(14)

The angular velocity of the rotor can be evaluated as follows:

$$\omega = \frac{v_0}{R_{\text{tire}}} = 157.89\ \text{rad/s}.$$
(15)

We used ANSYS Workbench software to determine the entire area of the disc friction track swept by the brake pads

during rotation while selecting on this contact surface that is equal to 35,797 mm^2, as it is shown in green color in Fig. 26.

Using the above calculations, the value of the hydraulic pressure P is obtained in the following form (Oder et al. 2009):

$$P = \frac{F_{\text{disc}}}{A_c\,\mu} = 1\ [\text{MPa}],$$
(16)

where μ is the friction coefficient, A_c is the surface of the brake pad in contact with the brake disc, which is obtained directly from simple selection in ANSYS Workbench. In
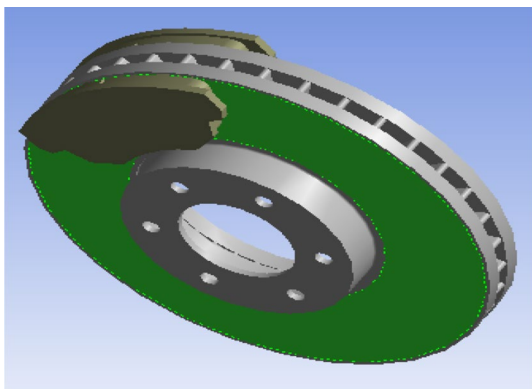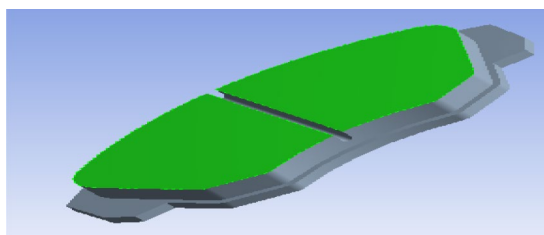
Fig. 26 Contact surface of the disc

Fig. 27 Contact surface of the pad

our case, it is indicated in green in Fig. 27 and equal to at 5246.3 mm^2.

9.2 Elastic problem

The mechanical stress is linked to the effort by a constitutive equation following:

$$\{\sigma\} = [D]\{\varepsilon^{\mathrm{me}}\}, \tag{17}$$

where $[D]$ is the material property matrix.

The total stress, sum of the mechanical and thermal stresses, is given by

$$\{\varepsilon\} = \{\varepsilon^{\mathrm{me}}\} + \{\varepsilon^{\mathrm{th}}\}, \tag{18}$$

where the upper indices (me) and (th) denote mechanical and thermal stresses, respectively,

Equation (17) becomes

$$\{\sigma\} = [D]\left\{\{\varepsilon\} - \{\varepsilon^{\mathrm{th}}\}\right\}, \tag{19}$$

where $\{\sigma\} = \{\sigma_r\,\sigma_\theta\,\sigma_z\,\sigma_{r\theta}\,\sigma_{\theta z}\,\sigma_{zr}\}$, $\{\varepsilon\} = \{\varepsilon_r\,\varepsilon_\theta\,\varepsilon_z\,\varepsilon_{r\theta}\,\varepsilon_{\theta z}\,\varepsilon_{zr}\}$.

For isotropic material, temperature change results in body expansion or shrinkage but no deformation. In other words, the temperature change affects the normal stresses without shear stresses.

The thermal stress vector is expressed as follows:

$$\{\varepsilon^{\mathrm{th}}\} = \{\alpha\,\Delta T\;\alpha\,\Delta T\;\alpha\,\Delta T\;0\;0\;0\},$$

where α is the coefficient of thermal expansion and ΔT indicates the temperature difference. Total stress is expressed in terms of nodal displacements as

$$\{\varepsilon\} = [B]\{d\}, \tag{20}$$

where $[B]$ is the kinematic matrix.

Substituting (20) in (19), we will have

$$\{\sigma\} = [D][B]\{d\} - [D]\{\varepsilon^{\mathrm{th}}\}. \tag{21}$$

The residual moment technique is applied to Eq. (21) and the results are found in the following equation:

$$[K]\{d\} = \{F^{\mathrm{th}}\} + \{F^{\mathrm{me}}\}, \tag{22}$$

where the elemental stiffness matrix for elasticity is given in the form:

$$[K^e] = \int_{\Omega^e} [B]^T[D][B]\,\mathrm{d}\,\Omega, \tag{23}$$

$\{F^{\mathrm{th}}\}$ and $\{F^{\mathrm{me}}\}$ are the thermal and mechanical force vectors that are denoted as follows:

$$\{F^{th}\} = \int_\Omega N^T N\,\mathrm{d}\,\Omega,$$

$$\{F^{\mathrm{me}}\} = \int_S N^T N\,\mathrm{d}\,S.$$

The elastic problem is solved by employing the constitutive equation. During numerical modeling, special attention is required to satisfy the continuity of normal displacements on the contact surface and the overlap conditions.

The following conditions of movement and effort are imposed on each pair of nodes on the interface:

$$W_i = W_j \text{ when } P > 0;\ W_i \neq W_j \text{ everywhere}, \tag{24}$$

$$\sigma_{zj} = -\sigma_{zj} \text{ when } P > 0;\ \sigma_{zj} \neq \sigma_{zj} \text{ everywhere}. \tag{25}$$

The following conditions of temperature and heat flux constraints are imposed on each pair of nodes on the interface:

$$T_i = T_j \text{ when } P > 0;\ T_i \neq T_j \text{ everywhere}, \tag{26}$$

$$q^* = \mu P \omega r \text{ when } P > 0;\ q^* = 0 \text{ everywhere}. \tag{27}$$

9.3 FE model and boundary conditions

The limit conditions applied to the model result from the assumptions and model choices presented above. Figure 28a, b shows the boundary conditions imposed on FE model,
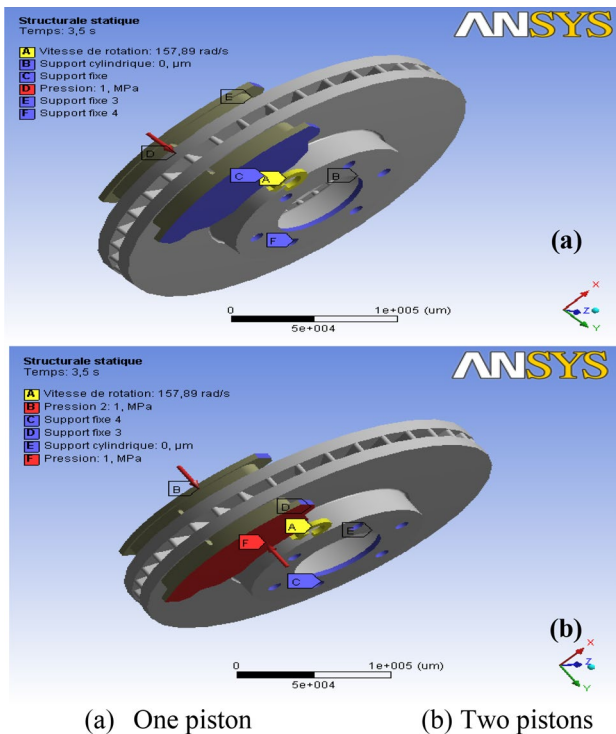
(a) One piston   (b) Two pistons

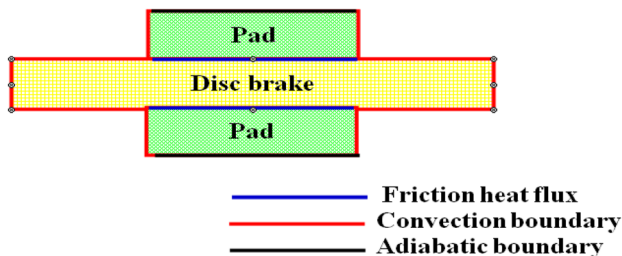**Fig. 28** Loading conditions for disc brake assembly

Fig. 29 Thermal boundary condition applied to the model

consisting of brake disc and two brake pads in dry contact in the case of pressure exerted on the one side of the pad and that of double pressure on both sides of the pad.

As we have done thermal analysis, the conditions to be taken into account are those which will influence the thermal phenomena such as the ambient temperature which is the initial temperature of disc 20 °C, the thermal flow and that of convection imposed on all the surfaces of the brake disc while for the two brake pads (Abu Bakar et al. 2010), convective heat exchange coefficient (*h*) of value 5 W/m^2 °C is applied on their outer surfaces on both sides (Fig. 29).

For structural boundary conditions, we know that the brake disc is fixed to the mounting holes thus requiring fixed support on these holes taking into account its rotational speed (Coudeyras 2009) $\omega = 157.89$ rad/s. The internal
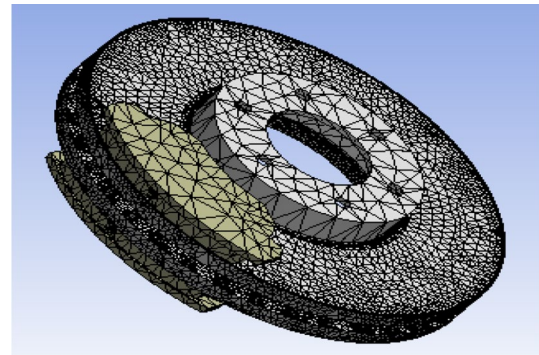

Fig. 30 Meshed model of disc brake assembly

disc diameter is sustained at fixed support for both radial directions while the tangential direction is left free in this simulation.

The structural boundary conditions applied to pads are also introduced. We imposed pressure of 1 MPa on the piston pad while maintaining fixed support on the finger pad while on the contact surface; the pad is assembled on its edges at the perpendicular plane. The friction between the two disc brake pad parts is defined by a coefficient equal to 0.2.

9.4 Geometry and mesh

Three-dimensional mesh of ventilated disc was developed under the ANSYS software (Fig. 30). The mesh is of three-dimensional tetrahedral type with 10 knots, regular on the tracks of friction and more and finer as one approach the surfaces of friction. The total number of nodes is 185,901 while the total number of elements is 113,367.

9.5 Thermal distortion

Figure 31 shows the maps of the total deformation of the whole model (disc brake pads) evaluated at times $t = 1.7271$ s, 3.5 s, 30 s and 45 s. According to this figure, the maximum total deformation recorded at time $t = 3.5$ s is of the order of 284.55 µm, where it coincides with the braking moment. It is obvious that strong distribution amplifies with time as well on the tracks of friction of the disc and its outer ring that its fins of cooling. Indeed, at the beginning of the braking, relatively homogeneous, relatively homogeneous, hot bands appear on the friction tracks of the disc. During braking, this hot strip with hot spots gradually migrates to the inner radius. Hot spots intensify to form stationary macroscopic hot spots at the inner radius. At the end of the braking, the intensity decreases and the surface gradients homogenize. The migration of the locations is explained by
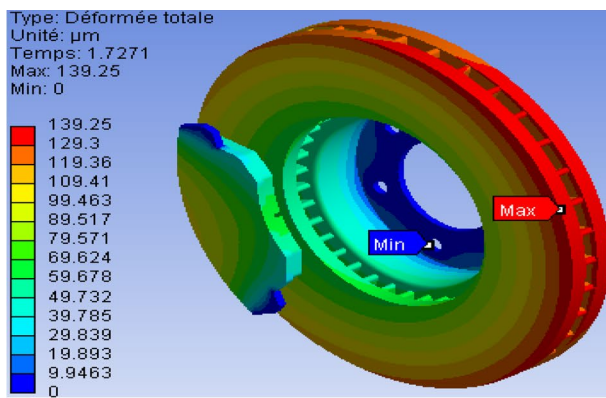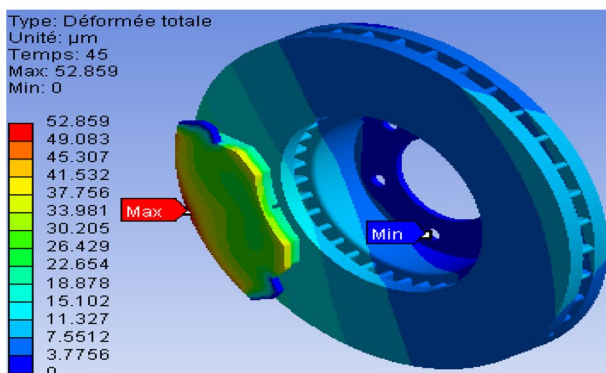
(a) t=1.7271 s
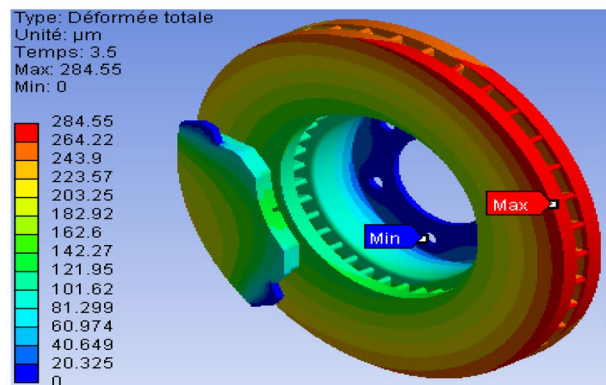
(b) t=3.5 s
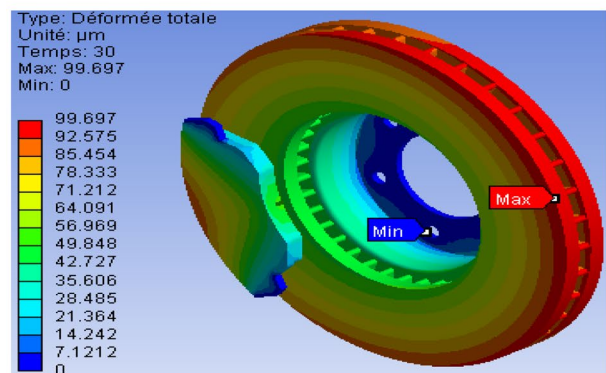
(c) t=30 s

(d) t=45 s

Fig. 31 Total deformation of disc–pad model

the difference in expansion between the track of the disc and its rear face, leading to "umbrella" deformed disc during warm-up. Deformation of the structure, therefore, has a preponderant role in the migration of thermal locations.

9.6 von Mises stress distribution

The model provides access to von Mises stress distribution mapping at the start of braking (Fig. 32) and after cooling the sector to ambient temperature. The distribution is well noted here in order ranging from 0 to 495.56 MPa. The great value recorded during this modeling in thermomechanical coupling is very significant when compared to mechanical dry contact analysis under the same braking conditions. According to the established conclusion, the von Mises stresses are maximums in the outer band at the level of the brake disc bowl at the instant 3.5 s, corresponding to the moment when the thermal gradient in the thickness of the track is the most important. Indeed, the brake disc is fixed to the hub by bolts to prevent its movement and as soon as it starts to rotate, torsion and shear stresses have just been produced at the level of its bowl which generates automatically stress concentrations around its fixing holes. The disc bowl thus risks mechanical rupture under repetitions of these undesirable effects during the braking process.

The general evolution of the stresses in the disc during the braking–cooling cycle is in agreement with the phenomena described in the previous literature searches.

9.7 Contact pressure distribution

Figure 33 shows mapping of the contact pressure at the friction interface between the internal brake pads and the brake disc with various simulation times. In these, the maximum contact pressures evaluated are of the order of 3.3477 MPa at the instant when the rotational speed is zero $t = 3.5$ s. It can also be seen that this maximum value is in the leading edges of the pads towards the trailing edge by friction. Moreover, the distribution of the contact pressure is quite symmetrical with respect to the groove of the brake pads. In the thermomechanical coupling that we carried out here, it is clear that the contact pressures are not negligible and can reach locally very high values, of the order of GPa. The plastic flow observed in the sliding direction attests well to the severity of the friction forces, so very high contact pressure.

9.8 von Mises stress at the inner pad

To study the influence of the groove of the brake pads as well as loading modes applied to the pistons (single pressure and double pressure). We solve the model and ask for the equivalent von Mises stress of three different designs. Brake pads in this case, brake pad with center groove
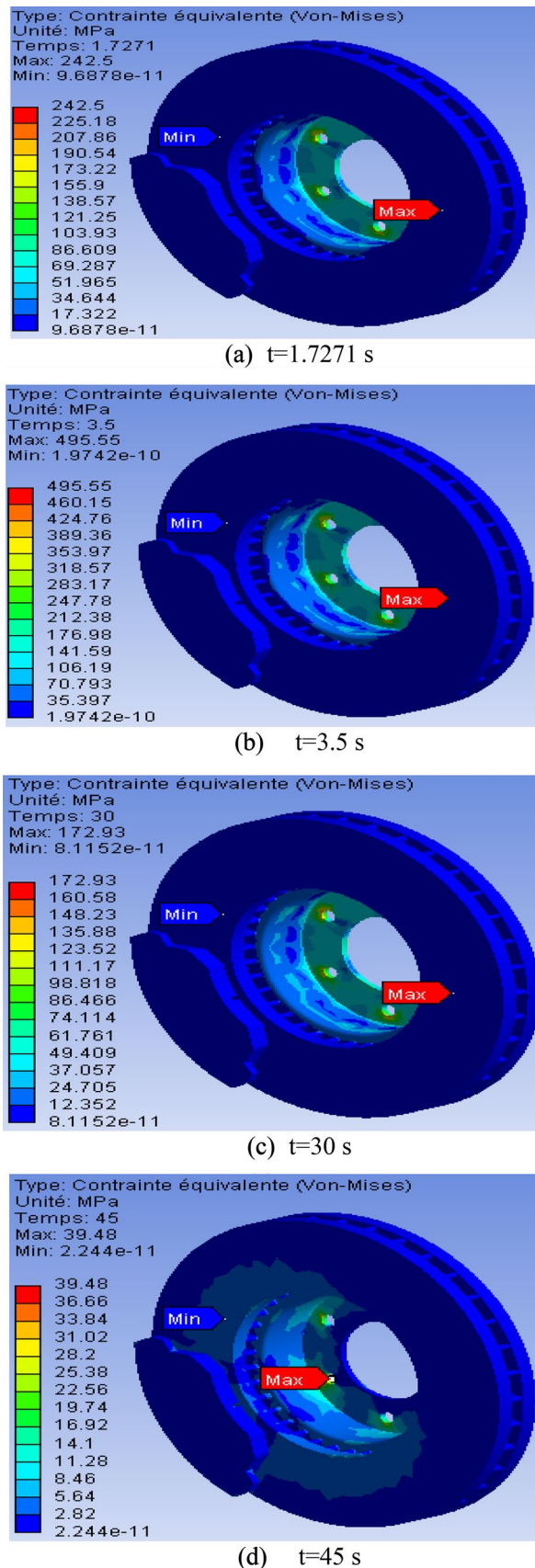
(a)	t=1.7271 s

(b)	t=3.5 s

(c)	t=30 s

(d)	t=45 s

Fig. 32 von Mises equivalent stress obtained step by step

(a)	t=1.7271 s	(b)	t=3.5 s
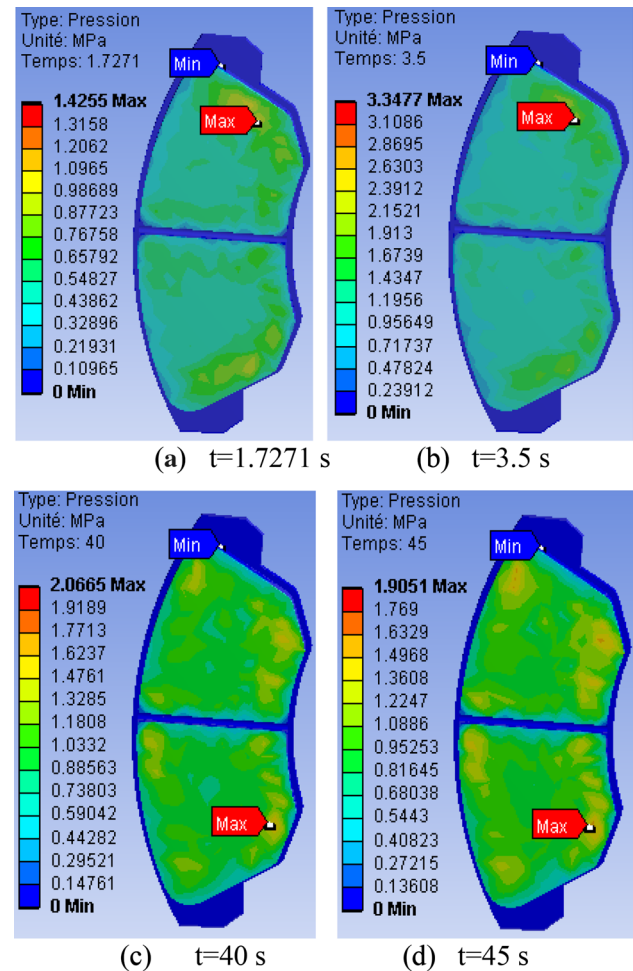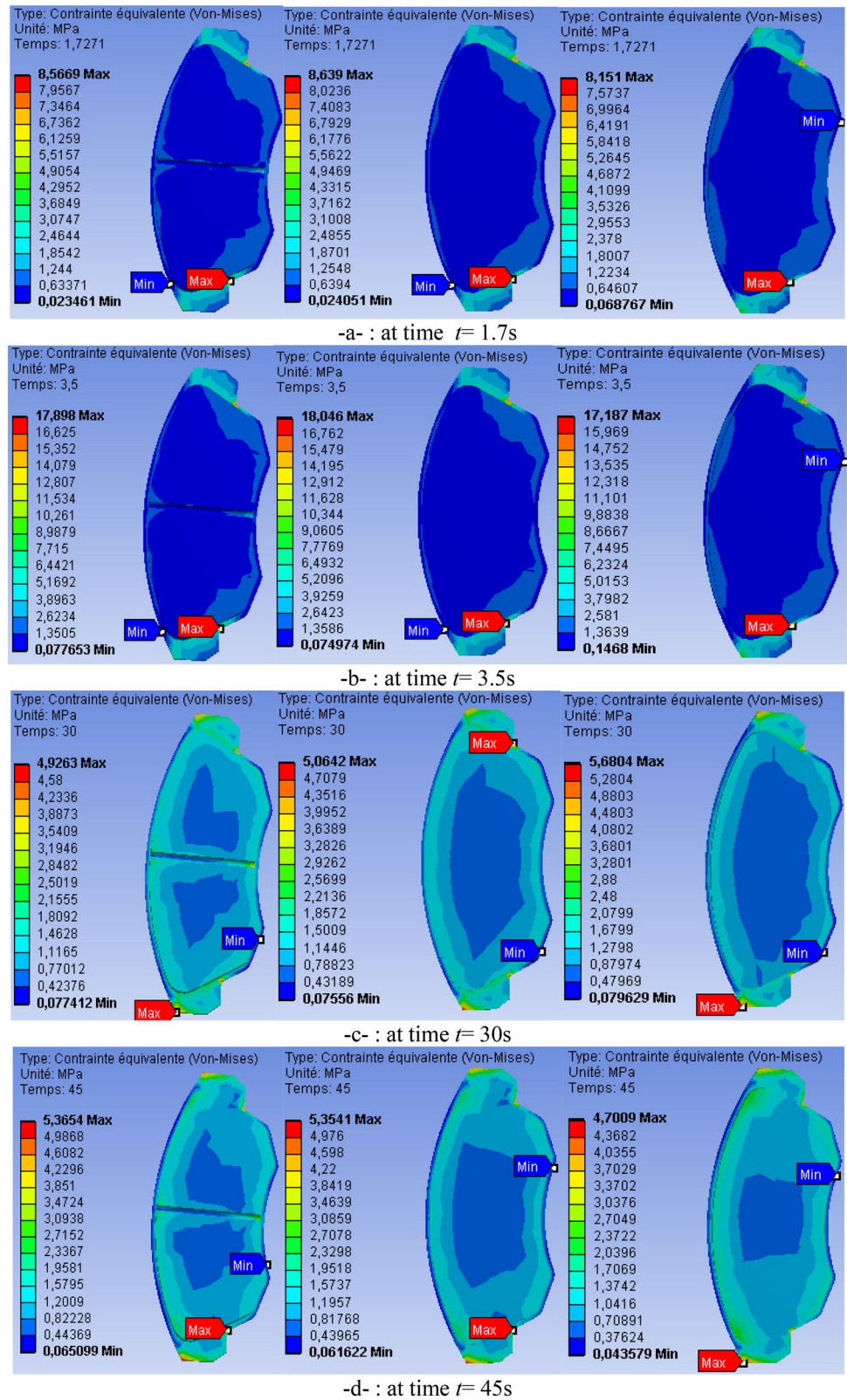
(c)	t=40 s	(d)	t=45 s

Fig. 33 Contact pressure distribution in the inner pad

subject to single double piston. We obtain the following visuals that are grouped in Fig. 34a–d. It can be seen that almost all the contact pads of the brake pads are dressed in dark blue color meaning low stresses at the beginning of the braking moment ($t = 1.7$ s). Nevertheless, from the moment of the end of braking $t = 45$ s, the scale of von Mises stress becomes more important whose vision of the colors becomes practically blue ocean whose distribution is well noticed on the three conceptions. It can be concluded that the existence of groove in brake pad and the presence of a mechanical double piston loading have positive influence on the distribution of brake pad stresses.

9.9 Validation of the thermomechanical model

To validate our thermomechanical model, we found in the literature, experimental test results and measurement that have been made by Abu Bakar (2005). For this reason, a comparison in contact pressure distribution of the inner pad was made between simulated and tested results.

Fig. 34 Distribution of von Mises stress at different braking time: Single piston with pad center groove (left), single piston without groove (center) and double piston without pad groove (right)

-a- : at time t= 1.7s

-b- : at time t= 3.5s

-c- : at time t= 30s

-d- : at time t= 45s

Fig. 35 A ventilated disc brake system

Fig. 36 Automotive use of break pressure sensor using Fujifilm Prescale® film before analysis

Fig. 37 An arrangement of brake pad surface measurements

We first briefly discussed the experimental procedure then we described the method of measurements used by this author to explain the investigation of the methodology to show the clarity of the idea.
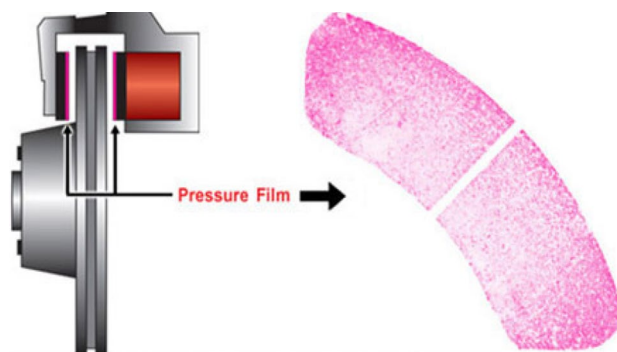
9.9.1 Experimental setup and contact pressure test

The contact pressure tests are conducted using an in-house disc brake dynamometer. The ventilated disc brake system of floating caliper design being investigated is shown in Fig. 35.

9.9.2 Pressurex® pressure-indicating film

Brake pressure sensors enable precision measurements of many critical performance and safety measurements under both normal and extreme operating conditions. Tactile brake pressure sensors can be used to detect the pressure distribution across many braking. A customized tactile brake pressure sensors enhanced with a robust optical analysis system can collect valuable data for a number of challenging automotive applications, to provide a complete pressure map. Fujifilm Prescale brake pressure sensor® is disposable and easy to employ, able to withstand demanding pressures and high temperatures. Using the Pressurex® Tactile indicating sensor film for clutch/brake applications is a cost-effective way to measure changes in pressure and distribution. Figure 36 presents usage of pressure film placed on a brake pad.

To measure contact pressure distributions, a suitable type of sensor film should be chosen for a particular range of local contact pressure. In this work, Pressurex® Super Low (SL) pressure-indicating film, which can accommodate contact pressure in the range of 1 MPa is selected. The film needs to be cut to the shape of the brake pad for it to be well positioned

in the pad/disc interface. Brake-line pressure at certain levels is then applied to the disc brake for 45 s and then removed.

9.9.3 Topaq® pressure analysis system

It is not quite sufficient to describe contact pressure distributions by showing only the stress marks on the tested films. The contact pressure distributions should be measured qualitatively and quantitatively for comprehensive understanding. In doing so, a system called Topaq® Pressure Analysis system is used. Topaq® is a revolutionary stress measurement instrument for analyzing force distribution and magnitude. Topaq's user-friendly Windows-based software enables the characterization of how force is disbursed in any process or assembly where two surfaces contact or impact.

A Mitutoyo linear gauge LG-1030E and digital scale indicator are used to measure and provide reading of the brake pad surface topography as shown in Fig. 37.

Figure 38 plots the comparison results and shows the significant variation of the two curves. The contact pressure distribution of the pads increases remarkably when the thermal and mechanical aspects are coupled.
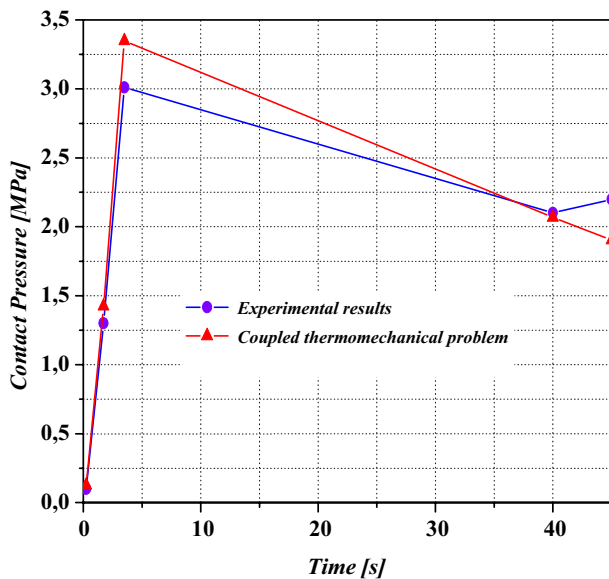
Fig. 38 Contact pressure of the inner pad

Also, it is clear from Fig. 38 that there is a good agreement between the numerical results and experimental data in thermomechanically coupled case. This gives an indication to brake engineers that to evaluate the brake performance, thermomechanical analysis should first be performed so that a realistic prediction can be achieved.

10 Conclusion

In the transport sector, braking is a major problem. It is question of obtaining on this safety equipment systematic reliability with acceptable cost, whereas the phenomena which are attached to it are complex.

In general, from the point of view of the thermal, the braking system is considered to be composed of only three elements: the disc in motion at variable speed, on which are rubbed the two pads which are subjected to pressure evolving over time. The phenomenon of induced friction generates dissipation of thermal power at the interface and will cause sharp increase in temperature which may deteriorate the equipment. The temperature level reached is directly related to the way in which the heat is transferred into its immediate environment, that is to say, the disc and the two pads.

In this paper, we presented complex modeling of convection-driven brake discs to predict the heat transfer coefficients (h) during the aerodynamic conditions of the braking stage using the software adapted in elements. ANSYS CFX finishes. Moreover, important results resulting from this numerical computation were used to study the transient thermal scenario during the braking and which was

executed on the two full and ventilated brake discs to which one visualized the temperature reached thanks to the software ANSYS Workbench. The main objective of this study is to unveil the system design impact of ventilation in the cooling mechanism of the brake discs to ensure famous thermal endurance that guarantees a longer life.

This research is conducted to study the relationship of the geometry of the brake disc with the better braking performance in terms of heat dissipation to the surroundings. From the results, it shows that ventilated disc brake has faster heat dissipation rate to surrounding compare to full disc brake. Thus, the ventilated disc brake is having better braking performance than full disc brake in terms of heat dissipation rate.

The results were also validated using the temperature–time profile from both the simulated and experimental results, in which the two results were found to be in good agreement. The literature for ventilated brake disc with gray cast iron FG15 also gives a good agreement with results from literature. In this research, we simulated the disc brake–pad assembly model by employing a coupled thermomechanical approach, whose results we obtained:

- At the level of outer radius and crown of disc, strong ditty occurs.
- In pad not containing groove and that subjected to double pressure, the stresses intensify significantly during braking.
- The temperature has a significant effect on the thermomechanical behavior of the braking system. Thus, in the presence of thermal effect, contact pressure of pad and overall, deformations of the brake disc are quite considerably prominent.

The temperature, stress, and total deformation of the disc and contact pressure of the pads rose due to the additional thermal stresses to the mechanical stresses, causing the cracks to propagate, the bowl to fracture, and the disc and pads to wear off. The numerical data obtained in this work also supported by the experimental results.

However, it seems to us that several thermomechanical turns can and should be visited in more detail in the topic of braking, essentially for more quantitative estimation of damage in life expectancy approach, which are defined in perspective. Additional thermomechanical speculations could be taken into consideration to better comment on the effect of migration of thermal locations.

Compliance with ethical standards

References

Abu Bakar AR (2005) Modelling and simulation of disc brake contact analysis and squeal." PhD Thesis, Department of Engineering, University of Liverpool, 2005

Abu Bakar AR, Ouyang H, Khai LC, Abdullah MS (2010) Thermal analysis of a disc brake model considering a real brake pad surface and wear. Int. J Veh Struct Syst 2(1):20–27

Adamowicz A, Grześ P (2012) Convective cooling of a disc brake during single braking. Acta Mechanica et Automatica 6(2):5–10

Belhocine A (2015) Numerical investigation of a three-dimensional disc-pad model with and without thermal effects. Therm Sci 19(6):2195–2204

Belhocine A, Bouchetara M (2012a) Thermomechanical modeling of dry contact in automotive disc brake. Int J Therm Sci 60:161–170

Belhocine A, Bouchetara M (2012b) Thermal behavior of full and ventilated disc brakes of vehicles. J Mech Sci Technol 26(11):3643–3652

Belhocine A, Ghazaly NM (2016) Effects of Young's modulus on disc brake squeal using finite element analysis. Int J Acoust Vib 31(3):292300

Belhocine A, Wan Omar WZ (2018) Predictive modeling and simulation of the structural contact problems between the brake pads and rotor in frictional sliding contact. Int J Interact Des Manuf 12(1):63–80

Belhocine A, Abu Bakar AR, Abdullah OI (2015) Structural and contact analysis of disc brake assembly during single stop braking event. Trans Indian Inst Met 68(3):403–410

Botkin ME (2000) Modelling and optimal design of a carbon fibre reinforced composite automotive roof. Eng Comput 16(1):16–23

Coudeyras N (2009) Non-linear analysis of multiple instabilities to the rubbing interfaces: application to the squealing of brake, PhD Thesis, Central school of Lyon-speciality: mechanics, December

Gotowicki PF, Nigrelli V, Mariotti GV, Aleksendric D, Duboka C (2005) Numerical and experimental analysis of a pegs-wing ventilated disk brake rotor with pads and cylinders. In: 10th EAEC Eur. Automot. Cong.–Paper EAEC05YUAS04–P5, June 2005

Huajiang O, Yuanxian G, Haitian Y (2004) A dynamic model for a disc excited by vertically misaligned, rotating, frictional sliders. Acta Mech Sin 20(4):418–442

Ishak MR, Abu Bakar AR, Belhocine A, Taib JM, Wan Omar WZ (2018) Brake torque analysis of fully mechanical parking brake system: theoretical and experimental approach. Ingenieria Investigacion y Tecnologia 19(1):37–49

Khalid MK, Mansor MR, Abdul Kudus SI, Tahir MM, Hassan MZ (2011) Performance investigation of the UTeM eco-car disc brake. Syst Int JEng Technol 11(6):1–6

Kothawade S, Patankar A, Kulkarni R, Ingale S (2016) Determination of heat transfer coefficient of brake rotor disc using CFD simulation. Int J Mech Eng Technol (IJMET) 7(3):276–284

Limpert R (1999) Brake design and safety, 2nd edn. Society of Automotive Engineering Inc., Warrendale, pp 137–144

Liu J, Ke LL, Wang YS (2019) Frictionally excited thermoelastic dynamic instability of functionally graded materials. Acta Mech Sin 35(1):99–111

Mackin TJ, Noe SC, Ball KJ, Bedell BC, Bim-Merle DP, Bingaman MC, Bomleny DM, Chemlir GJ, Clayton DB, Evans HA (2002) Thermal cracking in disc brakes. Eng Fail Anal 9:63–76

Oder G, Reibenschuh M, Lerher T, Šraml M, Šamec B, Potrč I (2009) Thermal and stress analysis of brake discs in railway vehicles. Adv Eng 3(1) (**ISSN 1846-5900**)

Palmer E, Mishra R, Fieldhouse JD (2009) An optimization study of a multiple row pin vented brake disc to promote brake cooling using computational fluid dynamics, Proc. Institution of Mech. Engineers, Part D, Journal of Automobile Engineering, 223(7): 865–875, 2009

Reimpel J (1998) Braking technology. Vogel Verlag, Würzburg

Stephens A (2006) Aerodynamic cooling of automotive disc brakes. Masters thesis. School of Aerospace, Mechanical & Manufacturing Engineering, RMIT University, March 2006

Tang J, Bryant D, Qi H (2014) Coupled CFD and FE thermal mechanical simulation of disc brake. In: Proc. Eurobrake Conference, Lille, France, 2014

Zhang J, Xia C (2012) Research of the transient temperature field and friction properties on disc brakes. In: Proceedings of the 2012 2nd international conference on computer and information application (ICCIA 2012), pp 201–204, 2012